Nonlinear transmission spectroscopy with dual frequency combs

Rachel Glenn and Shaul Mukamel
Department of Chemistry, University of California, Irvine, California 92697-2025, USA
(Received 18 April 2014; published 6 August 2014)

We show how two frequency combs $\mathcal{E}_1, \mathcal{E}_2$ can be used to measure single-photon, two-photon absorption (TPA), and Raman resonances in a molecule with three electronic bands, by detecting the radio frequency modulation of the nonlinear transmission signal. Some peaks are independent of the carrier frequency of the comb and others shift with that frequency and have a width close to the comb width. TPA and Raman resonances independent of the carrier frequency are selected by measuring the transmission signal $\sim \mathcal{E}_1^2\mathcal{E}_2^2$ and the single-photon resonances are selected by measuring the transmission signal $\sim \mathcal{E}_1^3\mathcal{E}_2$. Sinusoidal spectral phase shaping strongly affects the TPA, but not the Raman resonances.

DOI: 10.1103/PhysRevA.90.023804 PACS number(s): 42.62.Eh, 06.20.−f, 06.60.Jn, 42.65.Re

I. INTRODUCTION

Optical frequency combs, first introduced in 1999 [1], have revolutionized meterology [1,2] due to their high resolution of optical frequencies. They have been employed for calibrating sources of spectrographs in astronomy [3], identifying multiple molecules simultaneously [4], Doppler-free spectroscopy [5–7], improving energy efficiency in environmental monitoring [8], and forensic analysis, among its many applications. This technology has also enabled the generation of attosecond pulses [9]. Because the measurement times of the interferometric signal can be shortened from seconds using conventional pulse techniques, such as the scanning-arm Michelson interferometer [10], to microseconds with dual comb; future possible applications include the observation of chemical reactions in real time [11].

Dual-comb Fourier transform spectroscopy [8,12–17] is a technique employed for its spectral resolution and its concise recording times compared to conventional Fourier transform spectroscopy. It employees two coherent broadband optical frequency combs and records the nonlinear transmission in the time domain. A Fourier transformation reveals Raman resonances in the radio-frequency regime [13,15,18–23]. Previously, the spectrum was calculated numerically by means of calculating the intensity of light transmitted through an absorbing gas [20] or by means of fitting with the nonlinear least-squares method [18]. Here we calculate the nonlinear signal obtained with two frequency combs and connect them to the third-order susceptibility $\chi^{(3)}$. We address several issues: how the peaks map from the optical to the radio-frequency regime; how do the single-photon and two-photon resonances show up in the the transmission spectrum; how to selectively detect the two-photon absorption (TPA), Raman, and single-photon resonances in the transmission spectrum; and can we control these resonances by means of pulse-shaping?

We find the positions of some peaks are sensitive to the carrier frequency of the frequency comb, while other peaks not sensitive to carrier frequency. New peaks not studied previously [13,15,18–23] are calculated.

Pulse-shaping allows the control of the phase $\phi(\omega)$ and amplitude $\tilde{\mathcal{E}}(\omega)$ of the electric field $\mathcal{E}(\omega)$

$$\mathcal{E}(\omega) = \tilde{\mathcal{E}}(\omega)e^{i\phi(\omega)} \tag{1}$$

and has inspired the generation of arbitrary waveforms at optical frequencies [24–27]. We investigate how a sinusoidal phase added to the frequency comb affects the peaks in the spectrum.

This paper is organized as follows. In Sec. II we write the expressions for the nonlinear transmission spectrum. The transmission signal with of a Lorentzian pulse is plotted in Sec. III. The frequency comb in the time and frequency domains is presented in Sec. IV. The selection of the comb line numbers in the transmission spectrum and simulation of the transmission spectrum is given in Secs. V and VI. The comb transmission for a sinusoidal spectral phase is simulated in Sec. VII. The summary is presented in Sec. VIII.

II. NONLINEAR TRANSMISSION SIGNAL

We calculate the transmission signal measured in the time domain and Fourier-transformed to give the transmission spectrum [28]

$$S_t(\omega_s) = -\frac{2}{\hbar}\mathcal{I}\int dt e^{i\omega_s t}\mathcal{E}^*(t)P(t), \tag{2}$$

this yields

$$S_t(\omega_s) = -\frac{2}{\hbar}\mathcal{I}\int d\omega'\tilde{\mathcal{E}}^*(\omega'-\omega_s)P(\omega'), \tag{3}$$

where $P(\omega)$ is the polarization induced in the matter by the light and $\mathcal{I}A(\omega)$ denotes the imaginary part. The polarization will be expanded in powers of the radiation field [28]

$$P(\omega) = P^{(1)}(\omega) + P^{(3)}(\omega). \tag{4}$$

The first-order polarization is given by

$$P^{(1)}(\omega) = \mathcal{E}(\omega)\chi^{(1)}(\omega), \tag{5}$$

where $\chi^{(1)}(\omega)$ is the linear susceptibility. Inserting $P^{(1)}(\omega)$ into Eq. (3) gives

$$S_t^{(1)}(\omega_s) = -\frac{2}{\hbar}\mathcal{I}\int d\omega'\tilde{\mathcal{E}}^*(\omega'-\omega_s)\mathcal{E}(\omega')\chi^{(1)}(\omega'). \tag{6}$$

The third-order polarization is given as [28]

$$P^{(3)}(\omega) = \int d\omega_1 d\omega_2 d\omega_3 \mathcal{E}(\omega_1)\mathcal{E}(\omega_2)\mathcal{E}^*(\omega_3)\chi^{(3)} \times (-\omega;\omega_1,\omega_2,\omega_3)2\pi\delta(\omega-\omega_1-\omega_2+\omega_3), \quad (7)$$

where the susceptibility will depend upon the model of the system. Inserting Eq. (7) into Eq. (3) gives

$$S_t^{(3)}(\omega_s) = -\frac{2}{\hbar}\mathcal{I}\int d\omega' d\omega_1 d\omega_2 d\omega_3 \tilde{\mathcal{E}}^*(\omega'-\omega_s) \times \tilde{\mathcal{E}}(\omega_2)\tilde{\mathcal{E}}^*(\omega_3)\tilde{\mathcal{E}}(\omega_1)2\pi\delta(\omega'-\omega_1-\omega_2+\omega_3) \times \chi^{(3)}(-\omega',\omega_1,\omega_2,\omega_3). \quad (8)$$

Equation (8) will be used to calculate the transmission spectrum with a single broadband pulse and with a shaped-pulse composed of two frequency combs.

For comparison we also examine the heterodyne detected signal, i.e., transmission spectrum, measured in the frequency domain, called the frequency-dispersed transmission spectrum [28]

$$\mathcal{S}_f(\omega) = -\frac{2}{\hbar}\mathcal{I}\tilde{\mathcal{E}}^*(\omega)P(\omega). \quad (9)$$

Inserting Eq. (5), the first-order signal is given as

$$\mathcal{S}_f^{(1)}(\omega) = -\frac{2}{\hbar}\mathcal{I}|\tilde{\mathcal{E}}(\omega)|^2\chi^{(1)}(\omega). \quad (10)$$

Unlike Eq. (6), the signal does not depend upon the phase of the field.

Using Eq. (7), the third-order-dispersed spectrum is given as

$$\mathcal{S}_f^{(3)}(\omega) = \mathcal{I}\frac{2}{\hbar}\mathcal{E}^*(\omega)\int d\omega_1 d\omega_2 d\omega_3 \mathcal{E}(\omega_1)\mathcal{E}(\omega_2)\mathcal{E}^*(\omega_3) \times \chi^{(3)}(-\omega;\omega_1,\omega_2,\omega_3)2\pi\delta(\omega-\omega_1-\omega_2+\omega_3). \quad (11)$$

In the next section, we compare Eqs. (8) and (11) for a single pulse.

III. TRANSMISSION SIGNAL OF A BROADBAND PULSE

We consider a three-band model system Fig. 1 with electronic states $|g\rangle$, $|e\rangle$, $|f\rangle$. The linear susceptibility then reads [28]

$$\chi^{(1)}(\omega) = \sum_{e_1 g_1} -\frac{1}{\hbar}|\mu_{e_1 g_1}|^2 G_{e_1 g_1}(\omega), \quad (12)$$

where $G_{e_1 g_1}(\omega) = (\omega - \omega_{e_1 g_1} + i\Gamma_{e_1 g_1})^{-1}$.

The third-order susceptibility can be read off the diagrams of Fig. 2 [28]

$$\chi^{(3)}(-\omega;\omega_1,\omega_2,\omega_3) = \left(\frac{-1}{2\pi\hbar}\right)^3 \sum_{g_i,e_i,f_i} V_{g_1e_1}V_{e_1g_2}V_{g_2e_1}V_{e_1g_1}G_{e_1}^*(-\omega+\omega_1+\omega_2) \times G_{g_2}^*(-\omega+\omega_1)G_{e_1}(\omega_1) + V_{g_1e_1}V_{e_1f_1}V_{f_1e_1}V_{e_1g_1} \times G_{e_1}^*(-\omega+\omega_1+\omega_2)G_{f_1}(\omega_1+\omega_2)G_{e_1}(\omega_1) + V_{g_1e_1}V_{e_1g_2}V_{g_2e_1}V_{e_1g_1}G_{g_2}(\omega_1-\omega_3) \times G_{e_1}(\omega_1-\omega_3+\omega_2)G_{e_1}(\omega_1) + V_{g_1e_1}V_{e_1f_1}V_{f_1e_1}V_{e_1g_1} \times G_{e_1}(\omega_1+\omega_2-\omega_3)G_{f_1}(\omega_1+\omega_2)G_{e_1}(\omega_1). \quad (13)$$

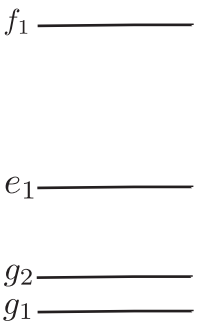

FIG. 1. The model level scheme contains three electronic states with the transition frequencies $\omega_{f_1g_1} = 36\,000\,\text{cm}^{-1}$, $\omega_{e_1g_1} = 12\,000\,\text{cm}^{-1}$, $\omega_{g_2g_1} = 1200\,\text{cm}^{-1}$. The dephasing rates are $\Gamma_{f_1g_1} = 500\,\text{cm}^{-1}$, $\Gamma_{e_1g_1} = 100\,\text{cm}^{-1}$, $\Gamma_{g_2g_1} = 80\,\text{cm}^{-1}$. The transition dipole moments are set to 1.

The frequency-dispersed transmission spectrum Eq. (11) with a Lorentzian pulse [29]

$$\mathcal{E}(\omega) = \frac{\sigma}{\omega + i\sigma} \quad (14)$$

is calculated analytically and shown in the top row of Fig. 3. $\mathcal{S}_f^{(3)}(\omega)$ is plotted in arbitrary units with the dipole moments set to 1. In Fig. 3(a), the resonances $\omega = \omega_{f_1e_1}, \omega_{e_1g_1}, \omega_{e_1g_2}$ are marked. The transmission spectrum contains the peaks $\omega = \omega_c - \omega_{g_2g_1}$, $\omega_{f_1g_1} - \omega_c$. The $\omega = \omega_{f_1g_1} - \omega_c$ peak overlaps with the $\omega = \omega_{e_1g_1}$ peak.

The dominant peak in the transmission spectra is the peak at the carrier frequency $\omega = \omega_c$. As the pulse width increases, in Fig. 3(b), the $\omega = \omega_{f_1g_1}, \omega_{e_1g_2}$ peaks become seen and the ω_c peak decreases. Increasing the pulse width further, Fig. 3(c), these peaks become more pronounced.

The Fourier transform of the time-resolved transmission signal Eq. (8) is shown the bottom row of Fig. 3 for the electric field (14). In Fig. 3(a), the two-photon transition $\omega_{f_1g_1}$ interacts two times with the pulse and it is shifted by $2\omega_c$. The single-photon transitions, $\omega_{e_1g_1}$, $\omega_{f_1e_1}$, interact once with the pulse and are shifted by ω_c. The Raman peaks are not shifted since they interact twice with the pulse, once with ω_c and a second with $-\omega_c$, which cancels. Increasing the pulse width to $\sigma = 500\,\text{cm}^{-1}$ in Fig. 3(e) the $\omega_s = \omega_{e_1g_1} - \omega_c$ peak remains dominant. This is also true for Fig. 3(b). Increasing the pulse width further, in Fig. 3(f) the peaks become smeared. Overall, the two signals $\mathcal{S}_f^{(3)}(\omega)$ and $S_t^{(3)}(\omega_s)$ are different.

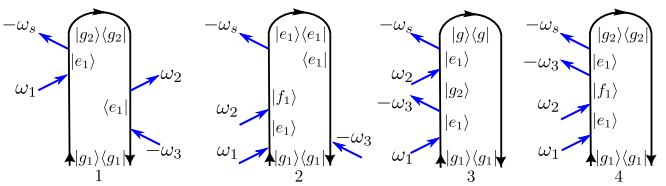

FIG. 2. (Color online) Loop diagrams for the transmitted signal Eq. (8) or Eq. (11).

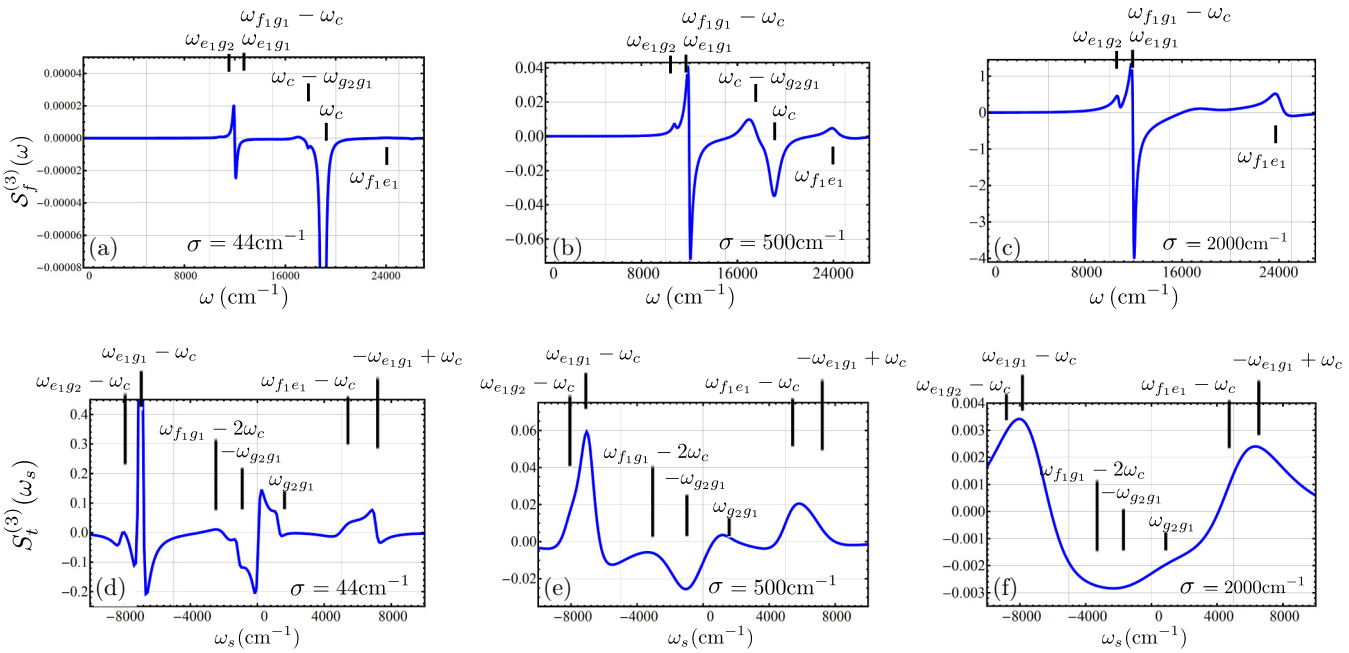

FIG. 3. (Color online) Top: The frequency-dispersed transmission spectrum $\mathcal{S}_f^{(3)}(\omega)$ Eq. (11) is plotted for a Lorentzian pulse Eq. (14), for several values of σ. Bottom: The Fourier transform of the time-resolved transmission signal $S_t^{(3)}(\omega_s)$ Eq. (8) is plotted for a Lorentzian pulse Eq. (14), for several values of σ. The signal is plotted in arbitrary units and the carrier frequency is $\omega_c = 19\,000\,\text{cm}^{-1}$. All dipole moments are set to 1.

IV. DUAL FREQUENCY COMB

The frequency comb is generated using a mode-locked laser that produces a series of optical pulses separated by the round-trip time of the laser cavity $T_{\text{rep}} = l_c/v_g$, where v_g is the group velocity and l_c is the round-trip length of the laser cavity [12,30–32]. We consider two femtosecond frequency combs, with the electric field $E(t) = \mathcal{E}(t) + \mathcal{E}^*(t)$

$$\mathcal{E}(t) = e^{-i\omega_c t}\sum_{n=1}^{N}\tilde{\mathcal{E}}(t - nT_{\text{rep},1})e^{-in(\Delta\phi - \omega_c T_{\text{rep},1})} + e^{-i\omega_c(t-\Delta t)}\sum_{n=1}^{N}\tilde{\mathcal{E}}(t - nT_{\text{rep},2} - \Delta t)e^{-in(\Delta\phi - \omega_c T_{\text{rep},2})}, \tag{15}$$

where ω_c is the carrier frequency and Δt is the delay between frequency combs. The summation index n represents the pulse number with a total of N pulses. The envelope function $\tilde{\mathcal{E}}(t)$ is periodic $\tilde{\mathcal{E}}(t) = \tilde{\mathcal{E}}(t + nT_{\text{rep}})$. The repetition frequencies are close, such that $\delta\omega_{\text{rep}} \ll \omega_{\text{rep},1}$, where $\delta\omega_{\text{rep}} = \omega_{\text{rep},1} - \omega_{\text{rep},2}$.

The carrier offset phase is $\omega_c T_{\text{rep},i}$. The phase $\Delta\phi = (1/v_g - 1/v_p)l_c\omega_c$, is the phase shift between the peak of the envelope and the closest peak of the carrier wave and v_p is the phase velocity. The range of the carrier-envelope phase is $0 < \Delta\phi < 2\pi$. It is possible to lock $\omega_c T_{\text{rep},i}$ to zero [31]. We assume a vanishing phase shift between pulses $\omega_c T_{\text{rep},i} + \Delta\phi = 0$.

The frequency comb can be generated by replacing the cavity with with a Fabry-Pérot etalon, [33]. In this method the individual pulse shape in the pulse train becomes asymmetric. An intracavity etalon is typically employed for self-stabilization of the optical frequencies and the pulse repetition rate in conventional frequency comb generation with high repetition rates 10 GHz [34]. An external molecular absorption cell can also be employed to stabilize the optical frequencies and the optical repetition rate [35].

An ideal frequency comb uses an infinite train of pulses ($N \to \infty$) and the electric field can be represented as a Fourier series

$$\mathcal{E}(t) = \mathcal{E}_1(t) + \mathcal{E}_2(t - \Delta t) = e^{-i\omega_c t}\sum_{n=-\infty}^{\infty}A_{n,1}e^{-in\omega_{\text{rep},1}t} + e^{-i\omega_c(t-\Delta t)}\sum_{m=-\infty}^{\infty}A_{m,2}e^{-im\omega_{\text{rep},2}(t-\Delta t)}, \tag{16}$$

where $\omega_{\text{rep},1} = 2\pi/T_{\text{rep},1}$ and $\omega_{\text{rep},2} = 2\pi/T_{\text{rep},2}$ and $A_{n,i}$ is the Fourier coefficient

$$A_{n,i} = \frac{1}{T_{\text{rep},i}}\int_{-\infty}^{\infty}\mathcal{E}_i(t)e^{-i(n\omega_{\text{rep},i} - \omega_c)t}dt, \tag{17}$$

$\mathcal{E}_i(t)$ is the pulse envelope, the index i represents comb 1 or comb 2.

The Fourier transform $\mathcal{E}(\omega) = \int_{-\infty}^{\infty}\tilde{\mathcal{E}}(t)e^{i\omega t}dt$ of Eq. (15) produces a frequency comb

$$\mathcal{E}(\omega) = \tilde{\mathcal{E}}(\omega - \omega_c)\sum_{n}^{N}e^{-in\omega T_{\text{rep},1} - in\Delta\phi} + \tilde{\mathcal{E}}(\omega - \omega_c)\sum_{m}^{N}e^{-im\omega T_{\text{rep},2} - im\Delta\phi - i\omega\Delta t} \tag{18}$$

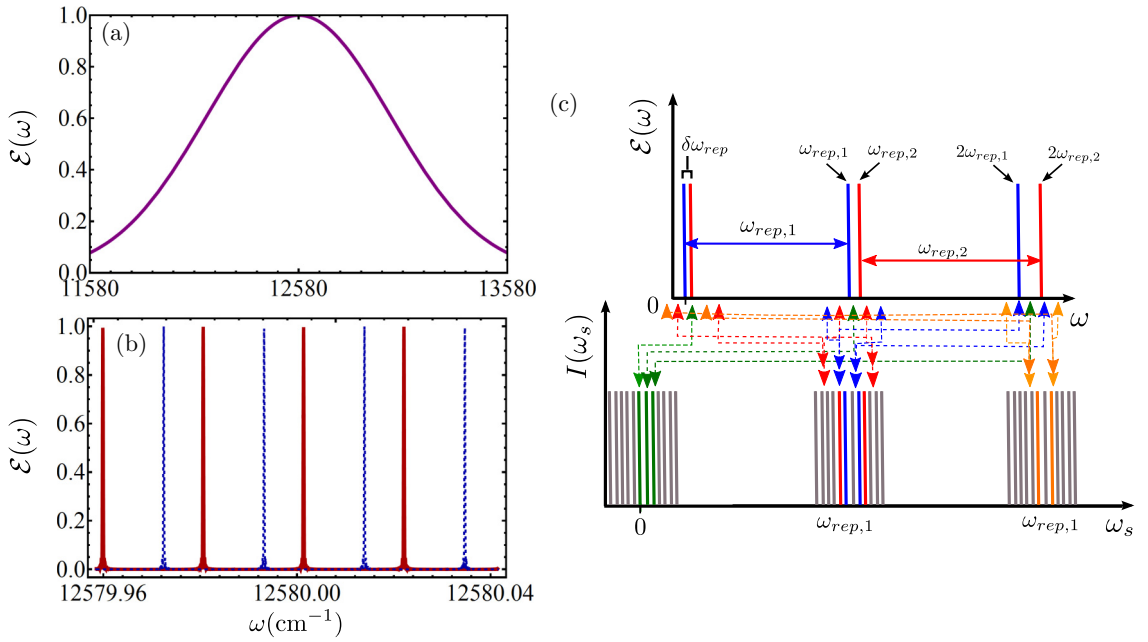

FIG. 4. (Color online) (a) Frequency comb, Eq. (18), for a Gaussian envelope Eq. (20) $\omega_{\mathrm{rep},1} = 0.0033\,\mathrm{cm}^{-1}$, $\eta = 10^{-6}$, $\omega_c = 12\,580\,\mathrm{cm}^{-1}$, and $\sigma = 441\,\mathrm{cm}^{-1}$. (b) The dual comb in (a) is displayed on a much smaller scale to that shown in the individual comb lines of comb 1 (dashed-blue line) and comb 2 (solid-red line). (c) Schematic of $\mathcal{E}(\omega)$ for the dual frequency comb Eq. (19). (d) Interferogram of the double comb Eq. (22) is shown for the first three frequency combs resulting from the beating of two frequency combs in the time domain.

with comb envelope $\tilde{\mathcal{E}}(\omega) = \int_{-\infty}^{\infty} \tilde{\mathcal{E}}(t) e^{-i\omega t} dt$. The summation of the exponentials in Eq. (18) is a Fourier series with constructive interference occurring at $\omega T_{\mathrm{rep},i} + \Delta\phi = 2\pi n$. The center frequency of line number n, with $\omega \to \omega_n$ is expressed as $\omega_n = n(1 - \frac{1}{2\pi}\Delta\phi)\omega_{\mathrm{rep},i}$. As the number of pulses N is increased the spectral width of the comb lines narrows and for $N \to \infty$ Eq. (18) can be simplified as

$$\mathcal{E}(\omega) = \omega_{\mathrm{rep},1}\tilde{\mathcal{E}}_1(\omega - \omega_c) \sum_{n=-\infty}^{\infty} \delta(n\omega_{\mathrm{rep},1} - \omega) + \omega_{\mathrm{rep},2}\tilde{\mathcal{E}}_2(\omega - \omega_c) e^{-i\omega\Delta t} \sum_{m=-\infty}^{\infty} \delta(m\omega_{\mathrm{rep},2} - \omega), \tag{19}$$

where we have selected $\Delta\phi = 0$. Equation (18) is plotted in Fig. 4 for a Gaussian envelope

$$\tilde{\mathcal{E}}_1(\omega - \omega_c) = E_1 e^{-(\omega-\omega_c)^2/2\sigma^2}, \quad \tilde{\mathcal{E}}_2(\omega - \omega_c) = E_2 e^{-(\omega-\omega_c)^2/2\sigma^2}, \tag{20}$$

with $\sigma = 441\,\mathrm{cm}^{-1}$, $\omega_c = 12\,580\,\mathrm{cm}^{-1}$, and for 100 pulses. Figure 4(a) shows the Gaussian envelope of the two overlapping frequency combs. There are 315,416 pulses contained in the full width half max (FWHM). Figure 4(b) shows the equidistant delta-like comb lines of the two frequency combs, in dashed-blue and solid-red, for $\omega_{\mathrm{rep},1} = 0.033\,\mathrm{cm}^{-1}$ and $\delta\omega_{\mathrm{rep}} = 10^{-6}\omega_{\mathrm{rep},1}$.

The beating of the two combs Eq. (16) creates a time-resolved interferometric signal $I(t) = |\mathcal{E}(t)|^2$, which reads

$$I(t) = |\mathcal{E}(t)|^2 = \sum_{p,r} A_{p,1}A^*_{r,1} e^{i(p-r)\omega_{\mathrm{rep},1}t} + \sum_{p,r} A_{p,2}A^*_{r,2} e^{i(p-r)\omega_{\mathrm{rep},2}(t+\Delta t)} + e^{-i\omega_c\Delta t} \sum_{n,m} A_{n,1}A^*_{m,2} e^{i(n\omega_{\mathrm{rep},1} - m\omega_{\mathrm{rep},2})t + im\omega_{\mathrm{rep},2}\Delta t} + e^{i\omega_c\Delta t} \sum_{n,m} A^*_{n,1}A_{m,2} e^{-i(n\omega_{\mathrm{rep},1} - m\omega_{\mathrm{rep},2})t - im\omega_{\mathrm{rep},2}\Delta t}. \tag{21}$$

The last two terms in Eq. (21) contain many possible beat frequencies: $n\omega_{\mathrm{rep},1} - m\omega_{\mathrm{rep},2}$. The Fourier transform of Eq. (21) reads

$$I(\omega_s) = \int dt\, I(t) e^{i\omega_s t}. \tag{22}$$

For $n = m$, Eq. (22) will give a frequency comb $\sum_n \delta(\omega_s - n\delta\omega_{\mathrm{rep}})$. The application of a second comb thus down-converts comb 1 by the factor

$$\eta = \delta\omega_{\mathrm{rep}}/\omega_{\mathrm{rep},1}. \tag{23}$$

This frequency comb has line spacing $\delta\omega_{\mathrm{rep}}$ and its envelope is the product of the envelopes of the two fields.

The dual frequency comb Eq. (19) is sketched in Fig. 4(c). Figure 4(c) sketches the Fourier transform of

the interferometric signal Eq. (21) given by Eq. (22). The first group of lines corresponds to the selection of the modes $n = m$. The second group corresponds to $m = n - 1$ and has the form $\sum_n \delta(\omega_s - \omega_{\mathrm{rep},2} - n\delta\omega_{\mathrm{rep}})$. It is centered at $\omega_s \approx \omega_{\mathrm{rep},1}$ with line spacing $\delta\omega_{\mathrm{rep}}$ and is identical to the first group. The third group is at $\omega_s \approx 2\omega_{\mathrm{rep},1}$ and corresponds to the combination $m = n - 2$. The spectrum contains an infinite number of identical frequency combs center at $\omega_s \approx p\omega_{\mathrm{rep},1}$, where p is an integer. Typically the only the first group of lines is measured and the higher frequencies can be cutoff experimentally by using a low-pass filter in the acquisition circuit [4]. For two combs with THz carrier frequencies, and repetition frequencies $\omega_{\mathrm{rep},1} = 2\pi$ 100 MHz, $\delta\omega_{\mathrm{rep}} = 2\pi 100$ Hz, the peaks in the spectrum are multiplied by $\eta = 10^{-6}$ and the spectrum lies in the radio-frequency regime [4]. For unambiguous assignment of the comb modes, the bandwidth should not exceed $\pm\omega_{\mathrm{rep},1}/2$, which can be derived from the Nyquist theorem.

V. COMB LINE SELECTION IN THE NONLINEAR TIME-RESOLVED TRANSMISSION SIGNAL WITH SCALING $\tilde{\mathcal{E}}_1^2\tilde{\mathcal{E}}_2^2$

The time-resolved transmission spectrum for two frequency combs contains the signals $\tilde{\mathcal{E}}_1^2\tilde{\mathcal{E}}_2^2$, $\tilde{\mathcal{E}}_1^3\tilde{\mathcal{E}}_2$, and $\tilde{\mathcal{E}}_1\tilde{\mathcal{E}}_2^3$. We analyze the spectrum separately for $\tilde{\mathcal{E}}_1^2\tilde{\mathcal{E}}_2^2$ and $\tilde{\mathcal{E}}_1^3\tilde{\mathcal{E}}_2$. For $\Delta t = 0$, the expression for the spectrum scaling as $\tilde{\mathcal{E}}_1\tilde{\mathcal{E}}_2^3$ are similar to $\tilde{\mathcal{E}}_1^3\tilde{\mathcal{E}}_2$ with the $\delta\omega_{\mathrm{rep}} \to -\delta\omega_{\mathrm{rep}}$.

We select terms that scale as $\tilde{\mathcal{E}}_1^2\tilde{\mathcal{E}}_2^2$. The Fourier transform of the interferometric signal with two interactions from combs 1 and 2, gives the following possible beat frequencies:

$$\begin{aligned}\omega_s &= (n-r)\omega_{\mathrm{rep},1} + (m-p)\omega_{\mathrm{rep},2}\\ &= (n+r)\omega_{\mathrm{rep},1} - (m+p)\omega_{\mathrm{rep},2}\\ &= (n-r)\omega_{\mathrm{rep},1} - (m-p)\omega_{\mathrm{rep},2}.\end{aligned} \tag{24}$$

Note that the exchange of $\omega_{\mathrm{rep},1}$ and $\omega_{\mathrm{rep},2}$ is possible in Eq. (24). The two interactions with comb 1 correspond the indices r and n, and two interactions with comb 2 to p and m. Similar to the interferometric signal Eq. (21), the relation $m - p = r - n$, for the first term in Eq. (24), will give a frequency comb $\sum_{n,r} \delta((n-r)\delta\omega_{\mathrm{rep}} - \omega_s)$. The combination $m - p = r - n + 1$ will give an identical frequency comb $\sum_{n,r} \delta((n-r)\delta\omega_{\mathrm{rep}} + \omega_{\mathrm{rep},2} - \omega_s)$, centered at $\omega_s \approx \omega_{\mathrm{rep},1}$. Based on this observation, we use a δ function to select the correct combination of line numbers. For example, the combination of the line numbers in Eq. (24) will acquire the corresponding δ functions

$$\begin{aligned}&\delta(n - r + m - p), \quad \delta(n + r - m - p),\\ &\delta(n - r - m + p),\end{aligned} \tag{25}$$

respectively. When expanding the field correlation functions we can insert the corresponding δ function and eliminate one of the summations over the spectral line numbers. This is done in Appendix A and the final expression for the time-resolved transmission spectrum is given in Eq. (A3).

The time-resolved transmission spectrum $S_t(\omega_s)$, Eq. (A3), contains many peaks. The TPA and Raman peaks that do not depend on n or m are

$$\begin{aligned}\omega_s &= \pm\eta\omega_{f_1g_1},\\ \omega_s &= \pm\eta\omega_{g_2g_1}.\end{aligned} \tag{26}$$

Other peaks that depend upon n and m and that lie within the displayed regime $\pm\omega_{\mathrm{rep},1}/2$ are

$$\begin{aligned}\tilde{\omega}^+_{f_1g_1} &= \eta\big[\omega_{f_1g_1} - (m+n)\omega_{\mathrm{rep},1}\big],\\ \tilde{\omega}^+_{e_1g_1} &= \eta\big(\omega_{e_1g_1} - n\omega_{\mathrm{rep},1}\big),\\ \tilde{\omega}^-_{e_1g_1} &= -\eta\big(\omega_{e_1g_1} + n\omega_{\mathrm{rep},1}\big),\\ \tilde{\omega}^+_{g_2g_1} &= \eta\big[\omega_{g_2g_1} - (m+n)\omega_{\mathrm{rep},1}\big],\\ \tilde{\omega}^-_{g_2g_1} &= -\eta\big[\omega_{g_2g_1} + (m+n)\omega_{\mathrm{rep},1}\big].\end{aligned} \tag{27}$$

The peaks $\omega_s = -\eta[\omega_{f_1g_1} + (m+n)\omega_{\mathrm{rep},1}]$, $\omega_{e_1g_1} \pm n\omega_{\mathrm{rep},1}$, $\omega_{g_2g_1} + (m+n)\omega_{\mathrm{rep},1}$ lie outside the displayed regime. The center position of the peaks that depend on n and m can be found by substituting $n = m = \omega_c/\omega_{\mathrm{rep},1}$. The single-photon peaks $\tilde{\omega}^-_{e_1g_1}$ and $\tilde{\omega}^+_{e_1g_1}$ depend on n; while, the range of n depends upon the width of the frequency comb. Hence, the width of these peaks will be close to the width of the frequency comb multiplied by η. The TPA and Raman resonances depend on m and n, so that these peaks will be twice as broad as the single-photon peaks.

The down-shifting of the peaks can be understood by comparing Eqs. (8) and (11). Equation (8) contains an ω' integration, which is a result of the time-resolved signal detection. This integration mixes the frequency combs and shifts the peaks into the radio-frequency range. Using the δ function in Eq. (8), and inserting it into the field $\tilde{\mathcal{E}}^*(\omega' - \omega_s)$, we find $\mathcal{E}^*(\omega_1 + \omega_2 - \omega_3 - \omega_s)$, which mixes the four frequencies in the diagrams of Fig. 2. In Eq. (11), using the δ function we have $\mathcal{E}^*(\omega_1 + \omega_2 - \omega_3)$, which mixes three of the frequencies.

The modulation of the transmission signal in the radio-frequency range, can be seen from the expression Eq. (A3), which is proportional to

$$\begin{aligned}S^{(3)}_{t1122}(\omega_s;\omega_{\mathrm{rep},1},\omega_{\mathrm{rep},2},\tau_2) \propto -\mathcal{I}\frac{2}{(2\pi\hbar)^4}\omega^2_{\mathrm{rep},1}\omega^2_{\mathrm{rep},2}\Big\{&\tilde{\mathcal{E}}^*_2(m\omega_{\mathrm{rep},2} - \omega_c)\tilde{\mathcal{E}}_1(n\omega_{\mathrm{rep},1} - \omega_c)\tilde{\mathcal{E}}^*_2(p\omega_{\mathrm{rep},2} - \omega_c)\\ &\times \tilde{\mathcal{E}}_1(r\omega_{\mathrm{rep},1} - \omega_c)V_{g_1e_1}V_{e_1f_1}V_{f_1e_1}V_{e_1g_1}\\ &\times \frac{\delta[(r+n)\omega_{\mathrm{rep},1} - (p+m)\omega_{\mathrm{rep},2} - \omega_s]}{\big(r\omega_{\mathrm{rep},1} - \omega_{e_1g_1} + i\Gamma_{e_1g_1}\big)\big[(n+r)\omega_{\mathrm{rep},1} - \omega_{f_1g_1} + i\Gamma_{f_1g_1}\big]\big[(n+r)\omega_{\mathrm{rep},1} - p\omega_{\mathrm{rep},2} - \omega_{e_1g_1} - i\Gamma_{e_1g_1}\big]}\end{aligned}$$

$$+\tilde{\mathcal{E}}_1^*(n\omega_{\mathrm{rep},1}-\omega_c)\tilde{\mathcal{E}}_2(m\omega_{\mathrm{rep},2}-\omega_c)\tilde{\mathcal{E}}_2^*(p\omega_{\mathrm{rep},2}-\omega_c)\tilde{\mathcal{E}}_1(r\omega_{\mathrm{rep},1}-\omega_c)V_{g_2e_1}V_{e_1g_1}V_{g_1e_1}V_{e_1g_2}$$
$$\times\frac{\delta[(r-n)\omega_{\mathrm{rep},1}-(p-m)\omega_{\mathrm{rep},2}-\omega_s]}{\big(r\omega_{\mathrm{rep},1}-\omega_{e_1g_1}+i\Gamma_{e_1g_1}\big)\big((p-m)\omega_{\mathrm{rep},2}-\omega_{g_2g_1}-i\Gamma_{g_2g_1}\big)\big(p\omega_{\mathrm{rep},2}-\omega_{e_1g_1}-i\Gamma_{e_1g_1}\big)}\Bigg\}. \quad (28)$$

The $\tilde{\mathcal{E}}_1^2\tilde{\mathcal{E}}_2^2$ scaling signal is designated as 1122. The first term

$$S^{(3)}_{t1122}(\omega_s)\propto\frac{\delta[(r+n)\omega_{\mathrm{rep},1}-(p+m)\omega_{\mathrm{rep},2}-\omega_s]}{\big[(n+r)\omega_{\mathrm{rep},1}-\omega_{f_1g_1}+i\Gamma_{f_1g_1}\big]}, \quad (29)$$

gives the two-photon peaks multiplied by η. Using $n+r=m+p$ in the δ function gives $(n+r)\delta\omega_{\mathrm{rep}}=\omega_s$. Substituting $(n+r)=\omega_s/\delta\omega_{\mathrm{rep}}$ into the denominator yields the TPA resonance at $\omega_s=\eta\omega_{f_1g_1}$. A similar effect occurs for the second term with the Raman resonances. From the combination of the terms

$$S^{(3)}_{t1122}(\omega_s)\propto\frac{\delta[(r-n)\omega_{\mathrm{rep},1}-(p-m)\omega_{\mathrm{rep},2}-\omega_s]}{\big[(p-m)\omega_{\mathrm{rep},2}-\omega_{g_2g_1}-i\Gamma_{g_2g_1}\big]}, \quad (30)$$

the selection $r-n=p-m$ in the δ function gives $(p-m)\delta\omega_{\mathrm{rep}}=\omega_s$. Substituting this combination into the dominator, we find the Raman resonance at $\omega_s=\eta\omega_{g_2g_1}$.

Two rather large summations are required to evaluate in the time-resolved transmission signal Eq. (A3). We performed them using the Monte Carlo method [36,37], where we randomly sample the comb line numbers in the frequency comb. Convergence is verified my changing the sample number and observing changes in the spectra.

The repetition frequency is selected as $\omega_{\mathrm{rep},1}=0.080\,\mathrm{cm}^{-1}$, so that the TPA peaks can be observed within the range $\pm\omega_{\mathrm{rep},1}/2$. The peaks in the transmission spectra are multiplied by the factor $\eta=10^{-6}$, which is in the radio-frequency range. We use a Gaussian envelope Eq. (20) with $\sigma=1.8\times10^6\,\mathrm{cm}^{-1}$.

The resonant time-resolved transmission signal Eq. (A3) is displayed in Fig. 5(a), for $\Delta t=0$, and $\omega_c=36\,000\,\mathrm{cm}^{-1}$. The comb bandwidth was selected as $\omega=(35\,000\,\mathrm{cm}^{-1},37\,000\,\mathrm{cm}^{-1})$ and contains 25 000 comb lines. The range was randomly sampled for 2000 pulses (dashed-red line) or 3500 pulses (solid-blue line). $S^{(3)}_{t1122}(\omega_s)$ is in arbitrary units with the dipole moments set to 1. The inset shows an illustration of the frequency comb used. The spectrum shows the TPA and Raman resonances at $\omega_s=\pm\eta\omega_{f_1g_1}$ and $\omega_s=\pm\eta\omega_{g_2g_1}$. The $\omega_s=\tilde{\omega}^+_{e_1g_1}$ peak is centered at $\omega_s=\eta(\omega_{e_1g_1}-\omega_c)=-24\,000\eta\,\mathrm{cm}^{-1}$ has a width $\approx2000\eta\,\mathrm{cm}^{-1}$. The $\omega_s=\tilde{\omega}^+_{f_1g_1}$ peak is located at $\omega_s=\eta(\omega_{f_1g_1}-2\omega_c)=-36\,000\eta\,\mathrm{cm}^{-1}$. Since its position depends on both n and m it will have a width of $\approx4000\,\eta\,\mathrm{cm}^{-1}$. This is the reason why

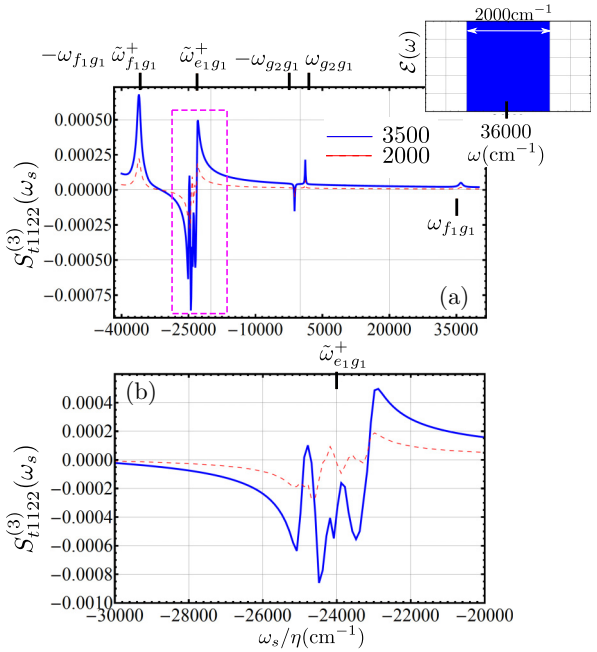

FIG. 5. (Color online) (a) The resonant time-resolved transmission spectrum from Eq. (A3) is plotted. Inset shows an illustration of frequency comb used $\omega_c=36\,000\,\mathrm{cm}^{-1}$ and bandwidth $2000\,\mathrm{cm}^{-1}$. (b) The spectrum near $\omega_s=\tilde{\omega}^+_{e_1g_1}$ is enlarged. The expression for the peaks are given in Eqs. (26) and (27).

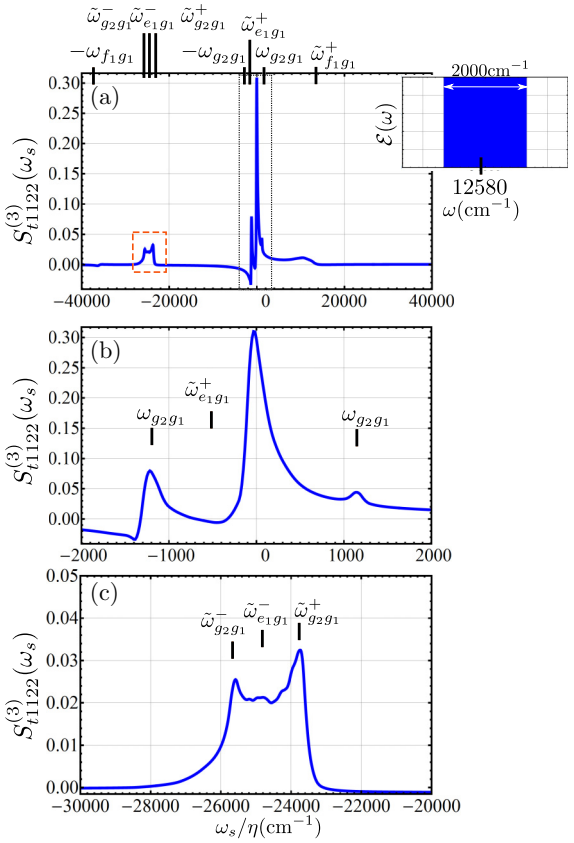

FIG. 6. (Color online) (a) The off-resonant time-resolved transmission spectrum. Inset shows a frequency comb centered at $\omega_c=12\,580\,\mathrm{cm}^{-1}$. (b) The spectrum about $\omega_s=0$ is enlarged. (c) The spectrum near $\omega_s=\tilde{\omega}^-_{e_1g_1}$ is enlarged. The expression for the peaks are given in Eqs. (26) and (27).

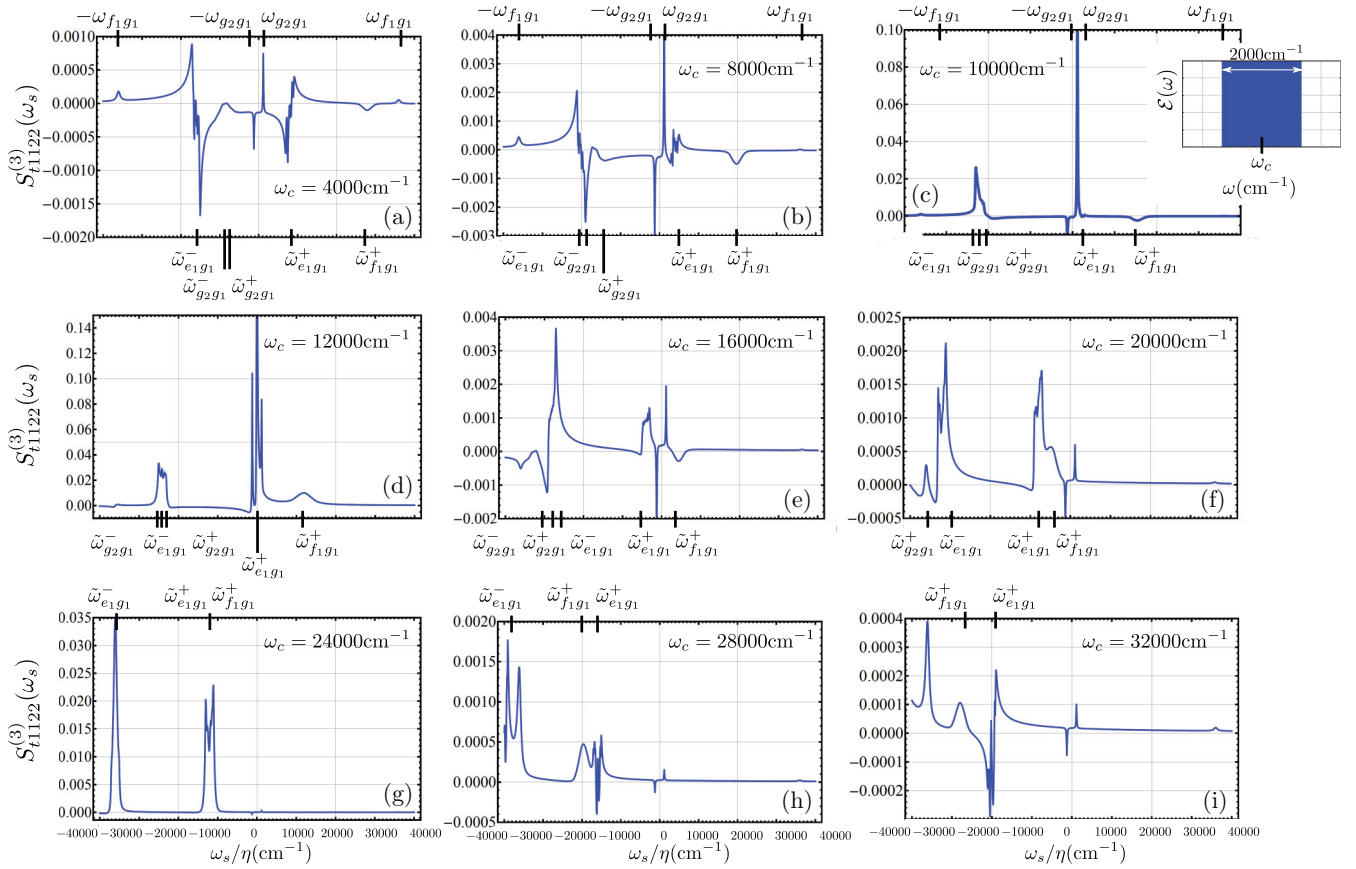

FIG. 7. (Color online) The time-resolved transmission spectrum $S^{(3)}_{t1122}(\omega_s)$ Eq. (A3) is displayed, for various values of ω_c. The inset shows the frequency comb centered at ω_c and width 2000 cm^{-1}. The expression for the peaks are given in Eqs. (26) and (27).

the negative two-photon peak in Fig. 5(a) is more pronounced than the positive peak.

The boxed region in Fig. 5(a) is replotted in Fig. 5(b) on a larger scale, which corresponds to $\omega_s = \tilde{\omega}^+_{e_1g_1}$. We see that the width of the peak is $\approx 2000\eta\,\text{cm}^{-1}$ and that it contains both absorption and emission features. Comparing the dashed-red line for 2000 sampled pulses to the solid-blue line 3500 pulses, we see the same features demonstrating that the data for the 2000 sampled pulses represents the spectrum.

The spectrum for $\omega_s > 0$ in Fig. 5(a), in the radio-frequency range, contains only the Raman and TPA peaks. Compared to the frequency-dispersed transmission spectra Fig. 3(c). Only the vibrational and TPA peaks are present in Fig. 5(b), while the Stokes, Rayleigh, single photon and TPA peaks are present in Fig. 3(c). In Figs. 5(a) and 3(d), the single-photon peaks are shifted by $\eta\omega_c$ or ω_c and there are Raman resonances not shifted by $\eta\omega_c$ or ω_c. In Fig. 5(a) there are TPA resonances that are not shifted by $2\eta\omega_c$ and in Fig. 3(d), they are shifted by $2\omega_c$.

The off-resonant transmission spectrum Eq. (A3) is shown in Fig. 6(a) for $\omega_c = 12\,580\,\text{cm}^{-1}$. The comb bandwidth was selected as $\omega = (11\,580\,\text{cm}^{-1}, 13\,580\,\text{cm}^{-1})$ and contains 25 000 comb lines. The range was randomly sampled for 2000 pulses. The TPA peaks are very weak. The spectrum is composed of Raman resonances at $\omega_s = \pm\eta\omega_{g_2g_1}$, $\tilde{\omega}^+_{g_2g_1}\tilde{\omega}^-_{g_2g_1}$, single-photon peaks at $\omega_s = \tilde{\omega}^+_{e_1g_1}, \tilde{\omega}^-_{e_1g_1}$, a TPA at $\omega_s = \tilde{\omega}^+_{f_1g_1}$, $-\eta\omega_{f_1g_1}$ and a peak at $\omega_s = 0$. The peak at $\omega_s = \tilde{\omega}^+_{f_1g_1} = 10\,840\eta\,\text{cm}^{-1}$ has a width of $\approx 4000\,\eta\,\text{cm}^{-1}$.

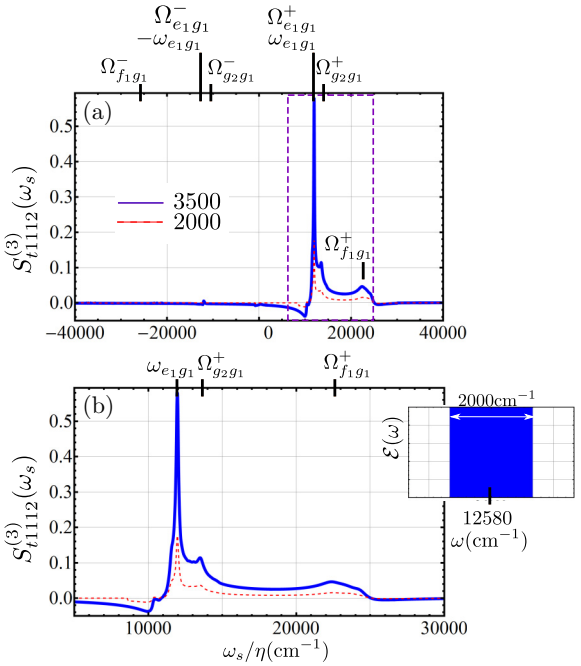

FIG. 8. (Color online) (a) The time-resolved transmission signal for three interactions with comb 1, Eq. (B3) is plotted. The inset shows an illustration of the frequency comb used, $\omega_c = 1258\,\text{cm}^{-1}$. The peaks in the spectrum are given by Eq. (32). (b) The spectrum in the purple-dashed region is replotted.

The region near $-24\,000\eta\ \mathrm{cm}^{-1}$ is replotted in Fig. 6(c) on an expanded scale and shows the combination of the peaks $\omega_s = \tilde{\omega}^-_{e_1g_1}$, $\tilde{\omega}^+_{g_2g_1}$, and $\tilde{\omega}^-_{g_2g_1}$, centered at $\omega_s = -24\,580$, $-23\,960$, $-26\,360\eta\ \mathrm{cm}^{-1}$, respectively.

The spectra near zero in Fig. 6(a), is replotted in Fig. 6(b). Compared to the resonant transmission spectrum Fig. 5(a), there is an additional peak at $\omega_s = 0$. This peak originates from $\omega_s = (\omega_{e_1g_1} - n\omega_{\mathrm{rep},1})$, which is not multiplied by the factor η. For $\omega_{e_1g_1} = n\omega_{\mathrm{rep},1}$, there is a peak which is located within the regime $\omega_{\mathrm{rep},1}/2$ at zero. The $\omega_s = \tilde{\omega}^+_{e_1g_1}$ peak is centered at $\tilde{\omega}^+_{e_1g_1} = -580\eta\ \mathrm{cm}^{-1}$, with width $\approx 2000\eta\ \mathrm{cm}^{-1}$.

The spectrum for $\omega_s > 0$ in Fig. 6(b) contains only the Raman peak. This plot can be compared to the experimental results of Ref. [4]. The spectrum shows qualitative agreement with there findings for measuring the off-resonant time-resolved transmission spectrum, without the peak at zero, which originates from the single-photon peak $\omega_s = (\omega_{e_1g_1} - n\omega_{\mathrm{rep},1})$. Note that we selected a different repetition frequency and level scheme Fig. 1 than the authors of Ref. [4].

The time-resolved transmission spectrum for various values of ω_c is plotted in Fig. 7. The inset shows the frequency comb that we use with bandwidth $2000\ \mathrm{cm}^{-1}$. The two large summations in Eq. (A3) are done by randomly sampling the range with 2000 pulses. The transmission spectrum for $\omega_c = 4000\ \mathrm{cm}^{-1}$ is shown in Fig. 7(a). It contains the two-photon and Raman resonances at $\omega_s = \pm\eta\omega_{f_1g_1}$, $\pm\eta\omega_{g_2g_1}$ and the five peaks in Eq. (27). The $\omega_s = \tilde{\omega}^+_{e_1g_1}$ and $\tilde{\omega}^-_{e_1g_1}$ peaks contain both absorption and emission features. The Raman peaks at $\omega_s = \tilde{\omega}^+_{g_2g_1}$ and $\tilde{\omega}^-_{g_2g_1}$ interfere. The $\omega_s = \tilde{\omega}^+_{f_1g_1}$ peak is an absorption peak. Increasing $\omega_c = 8000\ \mathrm{cm}^{-1}$, in Fig. 7(b), shifts the five peaks in Eq. (27) toward the left. In Fig. 7(c), for $\omega_c = 10\,000\ \mathrm{cm}^{-1}$ the $\omega_s = \tilde{\omega}^+_{e_1g_1}$ overlaps the $\omega_s = \pm\eta\omega_{g_2g_1}$ peak and amplifies the peak.

In the Fig. 7(d), for $\omega_c = 12\,000\ \mathrm{cm}^{-1}$, there is a peak located at zero, corresponding to $\omega_s = (\omega_{e_1g_1} - n\omega_{\mathrm{rep},1})$, which is not multiplied by the factor η. This peak only occurs for $\omega_{e_1g_1} = n\omega_{\mathrm{rep},1} = \omega_c$. In addition, the peak $\omega_s = \tilde{\omega}^+_{e_1g_1}$ is located at zero. Increasing ω_c further, in Fig. 7(f), the $\omega_s = \tilde{\omega}^-_{g_2g_1}$ position becomes located beyond the detected regime and all peaks from Eq. (27) are located in the regime $\omega_s < 0$. In Fig. 7(g), the $\tilde{\omega}^-_{e_1g_1}$ peak overlaps the TPA at $\omega_s = -\omega_{f_1g_1}$, amplifying the TPA. Increasing ω_c further, it is possible to shift the location of the $\omega_s = \tilde{\omega}^+_{g_2g_1}$ and $\tilde{\omega}^-_{e_1g_1}$ beyond the detected regime, as in Fig. 7(i).

VI. TIME-RESOLVED TRANSMISSION SIGNAL WITH SCALING $\tilde{\mathcal{E}}_1^3\tilde{\mathcal{E}}_2$

A selection of three interactions with comb 1 and one interaction with comb 2 will give the down-converted single-photon resonances, which do not depend upon the comb line number. The Fourier transform of the interferometric signal will give the following beat frequencies

$$\begin{aligned}\omega_s &= (n - r + m)\omega_{\mathrm{rep},1} - p\omega_{\mathrm{rep},2}\\ &= (n + r - m)\omega_{\mathrm{rep},1} - p\omega_{\mathrm{rep},2}\\ &= (n - r - m)\omega_{\mathrm{rep},1} + p\omega_{\mathrm{rep},2}.\end{aligned} \tag{31}$$

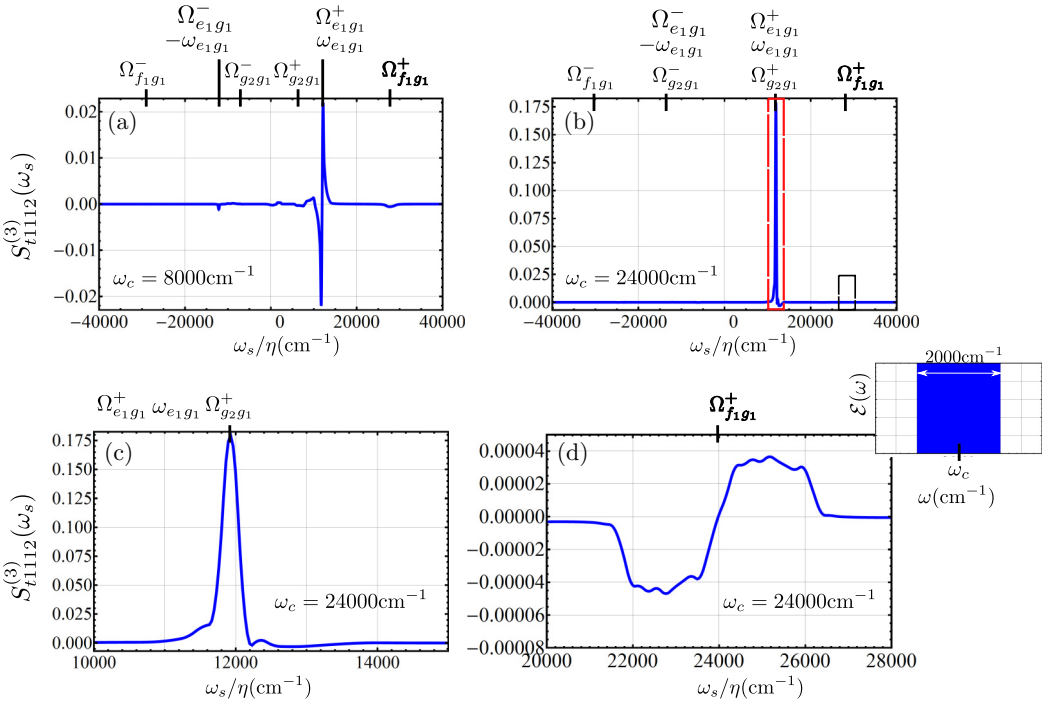

FIG. 9. (Color online) The time-resolved transmission signal for three interactions with comb 1, Eq. (B3) is plotted for two values of ω_c: (a) $\omega_c = 80\,000\ \mathrm{cm}^{-1}$, (b) $\omega_c = 240\,000\ \mathrm{cm}^{-1}$. The inset shows an illustration of the frequency comb used. The peaks in the spectrum given by Eq. (32). (c) The spectrum in the near $\omega_s = \eta\omega_{e_1g_1}$ is replotted. (d) The spectrum near $\Omega^+_{f_1g_1}$ is replotted.

Similar to the methods used in Sec. V, we will make use of a δ function to select the correct combination of line numbers in the transmission signal. The transmission spectrum Eq. (B3) is derived in Appendix B. The peaks in the transmission signal are

$$\begin{aligned}
\omega_{e_1g_1} &= \pm\eta\omega_{e_1g_1},\\
\Omega^{+}_{f_1g_1} &= \eta\big(\omega_{f_1g_1} - m\omega_{\mathrm{rep},1}\big),\\
\Omega^{-}_{f_1g_1} &= -\eta\big(\omega_{f_1g_1} - n\omega_{\mathrm{rep},1}\big),\\
\Omega^{+}_{e_1g_1} &= \eta\big[\omega_{e_1g_1} + (n-m)\omega_{\mathrm{rep}}\big],\\
\Omega^{-}_{e_1g_1} &= -\eta\big[\omega_{e_1g_1} - (n-m)\omega_{\mathrm{rep}}\big],\\
\Omega^{+}_{g_2g_1} &= \eta\big(\omega_{g_2g_1} + n\omega_{\mathrm{rep}}\big),\\
\Omega^{-}_{g_2g_1} &= -\eta\big(\omega_{g_2g_1} + m\omega_{\mathrm{rep}}\big).
\end{aligned} \tag{32}$$

The center position of the peaks can be found by substituting $n = \omega_c/\omega_{\mathrm{rep},1}$ and $m = \omega_c/\omega_{\mathrm{rep},1}$ into Eq. (32). The peak $\Omega^{\pm}_{e_1g_1}$ is centered at $\pm\omega_{e_1g_1}$. The peak positions $\Omega^{\pm}_{f_1g_1}$ are shifted by $-\eta\omega_c$, while, the peaks $\Omega^{\pm}_{g_2g_1}$ are shifted by $\eta\omega_c$. Comparing to the peaks in Fig. 3, the TPA peaks and Raman peaks in Fig. 3(c), $\mathcal{S}_f(\omega)$, are shifted by ω_c, while the single-photon peaks are not shifted by ω_c.

The down-conversion of the single-photon peaks can be seen from the transmission signal Eq. (B3), which is proportional to

$$\begin{aligned}
&S^{(3)}_{t1112}(\omega_s;\omega_{\mathrm{rep},1},\omega_{\mathrm{rep},2},\tau_2)\\
&\propto -\mathcal{I}\frac{2}{(2\pi\hbar)^4}\omega^3_{\mathrm{rep},1}\omega_{\mathrm{rep},2}\Big\{\tilde{\mathcal{E}}^*_1(m\omega_{\mathrm{rep},1}-\omega_c)\tilde{\mathcal{E}}_1(n\omega_{\mathrm{rep},1}-\omega_c)\tilde{\mathcal{E}}^*_2(r\omega_{\mathrm{rep},1}-\omega_c)\tilde{\mathcal{E}}_1(p\omega_{\mathrm{rep},2}-\omega_c)V_{g_1e_1}V_{e_1g_2}V_{g_2e_1}V_{e_1g_1}\\
&\times\frac{\delta[(n-r-m)\omega_{\mathrm{rep},1}+p\omega_{\mathrm{rep},2}-\omega_s]}{\big(p\omega_{\mathrm{rep},2}-\omega_{e_1g_1}+i\Gamma_{e_1g_1}\big)\big(p\omega_{\mathrm{rep},2}-r\omega_{\mathrm{rep},1}-\omega_{g_2g_1}+i\Gamma_{g_2g_1}\big)\big[(n-r)\omega_{\mathrm{rep},1}+p\omega_{\mathrm{rep},2}-\omega_{e_1g_1}-i\Gamma_{e_1g_1}\big]}\Big\},
\end{aligned} \tag{33}$$

The index 1112 represents the signal scaled as $\tilde{\mathcal{E}}^3_1\tilde{\mathcal{E}}_2$. Equation (33) is proportional to

$$\begin{aligned}
&S^{(3)}_{t1112}(\omega_s;\omega_{\mathrm{rep},1},\omega_{\mathrm{rep},2},\tau_2)\\
&\propto\frac{\delta[(n-r-m)\omega_{\mathrm{rep},1}+p\omega_{\mathrm{rep},2}-\omega_s]}{\big(p\omega_{\mathrm{rep},2}-\omega_{e_1g_1}+i\Gamma_{e_1g_1}\big)}.
\end{aligned} \tag{34}$$

The selection $n-r-m=-p$ from the measurement of interferometric signal gives $p=-\omega_s/\delta\omega_{\mathrm{rep}}$. Substituting this into the dominator we find the single-photon resonance at $\omega_s=-\eta\omega_{e_1g_1}$.

The two large summations in the transmission signal $S^{(3)}_{t1112}(\omega_s)$ are calculated using the Monte Carlo method, as in Sec. V. We used the same values for the repetition frequency and Gaussian pulse width as in Sec. V. The off-resonant transmission signal is displayed for $\omega_c = 12\,580\,\mathrm{cm}^{-1}$ and a comb bandwidth $\omega = (11\,580\,\mathrm{cm}^{-1}, 13\,580\,\mathrm{cm}^{-1})$ in Fig. 8. The inset shows an illustration of the frequency comb used. The range was randomly sampled for 2000 pulses (dashed-red line) and 3500 pulses (solid-blue line). $S^{(3)}_{t1112}(\omega_s)$ is in arbitrary units with the dipole moments set to 1. The transmission spectrum in Fig. 8(a) is dominated by the $\omega_s=\omega_{e_1g_1}$ peak. The $\omega_s=\Omega^{+}_{e_1g_1}$ peak has a width of 4000 $\eta\,\mathrm{cm}^{-1}$ and overlaps the $\omega_s=\omega_{e_1g_1}$ peak. The $\omega_s=\Omega^{+}_{f_1g_1}$ peak has a width of $2000\eta\,\mathrm{cm}^{-1}$. Comparing the 2000 sampled to the 3500 sampled, the features from the 2000 pulses resemble the 3500. The boxed region is replotted in Fig. 8(b) on a smaller regime. The $\omega_s=\Omega^{+}_{g_2g_1}$ has a width of $2000\,\mathrm{cm}^{-1}$. There is a feature near $\omega_s=-10\,000\eta\,\mathrm{cm}^{-1}$ that corresponds to the $\omega_s=\Omega^{+}_{e_1g_1}$ peak.

The transmission signal for two values of ω_c are shown in Fig. 9. For $\omega_c<\omega_{e_1g_1}$ in Fig. 9(a), the spectrum is mostly composed of the single-photon peak, which shows both emission and absorption features. For $\omega_c>\omega_{e_1g_1}$, in Fig. 9(b), the single-photon peak becomes an emission peak and all peaks dependent upon comb line number are suppressed. There are three peaks, $\omega_s=\omega_{e_1g_1}$, $\Omega^{+}_{g_2g_1}$, $\Omega^{+}_{e_1g_1}$ that overlap. The spectrum near $\omega_s=\eta\omega_{e_1g_1}$ is replotted in Fig. 9(c), showing that the single-photon resonance has width according to the dephasing rate. The peak at $\Omega^{+}_{f_1g_1}$, is plotted in Fig. 9(d).

VII. TIME-RESOLVED TRANSMISSION SPECTRA WITH SHAPED SPECTRAL PHASE

The future developments in spectroscopy using the frequency comb include shaping the individual pulses in the pulse train. This method requires a pulse shaper to have a spectral resolution that matches the spacing of the comb lines of the input pulse train. This was demonstrated recently [24,26,38–40]. Currently, this method is limited to small frequency combs, say 100 comb lines. The generation of pulse shaping in dual comb Fourier transform spectroscopy was recently demonstrated for triangular shaped pulses [25]. The two frequency combs contained four identically shaped pulses with slightly different repetition rates. Here, we consider the pulse shaping of a frequency comb with 25 000 pulses using a sinusoidal spectral phase function. This was demonstrated in Doppler free spectroscopy [6] with a repetition frequency of 180 MHz ($0.06\,\mathrm{cm}^{-1}$).

The spectrum with two interactions with comb 1 $S^{(3)}_{t1122}(\omega)$ contains the peaks $\omega_s=\pm\eta\omega_{g_2g_1}$ and $\omega_s=\pm\eta\omega_{f_1g_1}$ that are independent of the comb line numbers. We are interested in controlling these resonances by means of employing an oscillating phase onto the pulse envelope

$$\tilde{\mathcal{E}}_1(\omega)=\mathcal{E}_1(\omega)e^{i\phi(\omega)},\quad \tilde{\mathcal{E}}_2(\omega)=\mathcal{E}_2(\omega)e^{i\phi(\omega)}, \tag{35}$$

where $\mathcal{E}_1(\omega)$ and $\mathcal{E}_2(\omega)$ represent the real part, which is a Gaussian, Eq. (20). The sinusoidal spectral phase reads

$$\phi(\omega)=\alpha\sin(\beta\omega+\Phi), \tag{36}$$

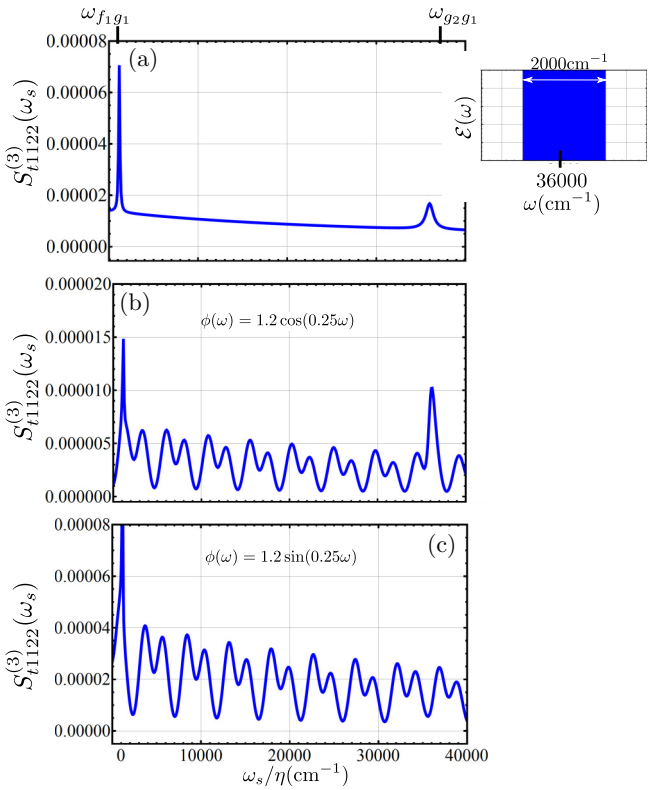

FIG. 10. (Color online) (a) The resonant time-resolved transmission signal Eq. (A3) without a sinusoidal phase. The resonant transmission signal Eq. (A3) using Eq. (35), with an oscillating phase Eq. (36), for $\beta = 0.25$, $\alpha = 1.2$, and two different values of the Φ; (a) $\Phi = \pi/2$; (b) $\Phi = 0$. The inset in (a) shows the frequency comb used.

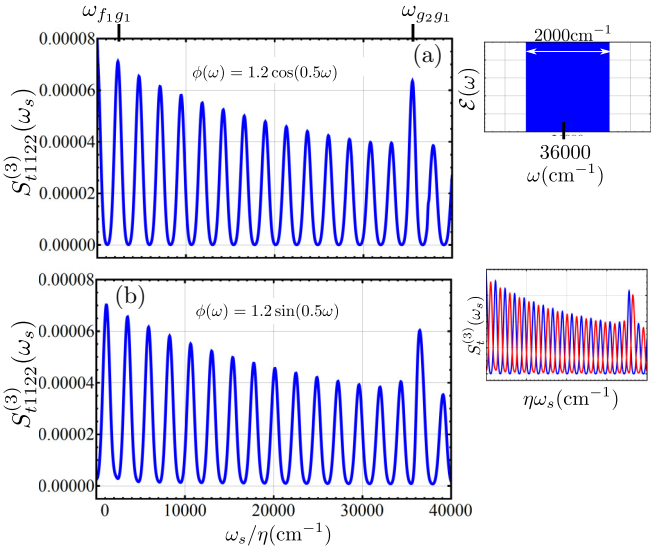

FIG. 11. (Color online) The resonant time-resolved transmission signal Eq. (A3) for $\beta = 0.5$, $\alpha = 1.2$, and two different values of the Φ in Eq. (36). (a) $\Phi = \pi/2$; (b) $\Phi = 0$. The inset in (a) shows the frequency comb used.

where α is the modulation depth, β is inverse modulation frequency, and Φ is the modulation phase. A cosine spectral phase occurs when $\Phi = \pi/2$. Adding an oscillating phase alters the temporal profile, breaking each pulse into a train of subpulses.

In Fig. 10(a), we show the time-resolved transmission spectrum, without an oscillating phase, for $\omega_c = 36\,000\,\text{cm}^{-1}$ and bandwidth $\omega = (35\,000\,\text{cm}^{-1}, 37\,000\,\text{cm}^{-1})$. See the inset. For an even spectral phase Fig. 10(b), $\Phi = \pi/2$, both the Raman and TPA peaks are present. However, for an odd spectral phase Fig. 10(c), $\Phi = 0$, only the Raman peak is present.

The suppression of the Raman peak can be done by selection of the modulation frequency β. In Fig. 11(a), for an even phase function, the Raman peak in the spectrum is minimized while the TPA peak is enhanced. The minimization of the Raman peak is not do to a minimum in the oscillating spectral phase function. This is verified in Fig. 11(b), where we plot the transmission spectrum with an odd phase function $\Phi = 0$. The inset, which is a plot of Figs. 11(c) and 11(d), demonstrates that the cosine and sine spectral phase functions are out of phase.

VIII. SUMMARY

We have shown that dual comb spectroscopy can be described as the time-resolved transmission signal of single shaped pulse. The selection of the combination of the comb line numbers in the frequency comb leads to Raman, TPA, and single-photon resonances in the radio-frequency regime.

For a single broadband pulse, the single-photon peaks were shifted by ω_c. The TPA were shifted by $2\omega_c$ and the Raman peaks are not shifted. For the dual comb, there are several peaks in the spectrum. The time-resolved transmission signal proportional to $\tilde{\mathcal{E}}_1^2\tilde{\mathcal{E}}_2^2$ gives single-photon peaks shifted by $\eta\omega_c$. The TPA and Raman resonances have several peaks in the spectrum. First, the peaks that are not shifted by $\eta\omega_c$ and have a width equal to the dephasing rate. Second, the peaks that are shifted by $2\eta\omega_c$ with a width proportional to the width of the frequency comb. It is the selection of the comb lines which allows some of the TPA and Raman resonances to not be shifted by $\eta\omega_c$.

The $\tilde{\mathcal{E}}_1^3\tilde{\mathcal{E}}_2$ time-resolved transmission signal gives TPA and Raman resonances shifted by $\eta\omega_c$. There are two types of single-photon resonances: peaks that have a width dependent upon the width of the frequency comb and peaks with linewidths according to the dephasing rate.

For a frequency comb, with several hundred thousand comb lines, the time-resolved transmission spectra will be composed of the TPA and Raman or single-photon resonances, which are not shifted by $\eta\omega_c$. For a small frequency comb, with one or two comb lines, the spectra will be composed mostly of the peaks which are shifted by $\eta\omega_c$.

ACKNOWLEDGMENTS

We gratefully acknowledge the support of the National Science Foundation (Grant No. CHE-1361516) and the Chemical Sciences, Geosciences, and Biosciences Division, Office of Basic Energy Sciences, Office of Science, US Department of Energy.

APPENDIX A: TIME-RESOLVED TRANSMISSION SIGNAL $\tilde{\mathcal{E}}_1^2\tilde{\mathcal{E}}_2^2$

Using Eq. (19) and the corresponding δ functions in Eq. (25), the transmission signal Eq. (8) can be cast into the following form:

$$\begin{aligned}
S^{(3)}_{t1122}(\omega_s;\omega_{\mathrm{rep},1},\omega_{\mathrm{rep},2},\Delta t) = -\mathcal{I}\frac{2}{\hbar}\omega^2_{\mathrm{rep},1}\omega^2_{\mathrm{rep},2}\int_{-\infty}^{\infty}d\omega_1\int_{-\infty}^{\infty}d\omega_2\int_{-\infty}^{\infty}d\omega_3 \\
\times [\tilde{\mathcal{E}}_1^*(\omega_1+\omega_2-\omega_3-\omega_s;n\omega_{\mathrm{rep},1})\tilde{\mathcal{E}}_2(\omega_2;m\omega_{\mathrm{rep},2})\tilde{\mathcal{E}}_2^*(\omega_3;p\omega_{\mathrm{rep},2})\tilde{\mathcal{E}}_1(\omega_1;r\omega_{\mathrm{rep},1})\delta(n-r-m+p) \\
\times e^{i(\omega_2-\omega_3)\Delta t} + \tilde{\mathcal{E}}_2^*(\omega_1+\omega_2-\omega_3-\omega_s;m\omega_{\mathrm{rep},2})\tilde{\mathcal{E}}_1(\omega_2;n\omega_{\mathrm{rep},1})\tilde{\mathcal{E}}_1^*(\omega_3;r\omega_{\mathrm{rep},1})\tilde{\mathcal{E}}_2(\omega_1;p\omega_{\mathrm{rep},2}) \\
\times \delta(-n+r+m-p)e^{-i(\omega_2-\omega_3-\omega_s)\Delta t}][\chi^{(3)}(-\omega_1-\omega_2+\omega_3;\omega_1,\omega_2,\omega_3) \\
+ \chi^{(3)}(-\omega_1-\omega_2+\omega_3;\omega_2,\omega_1,\omega_3)] + [\tilde{\mathcal{E}}_1^*(\omega_1+\omega_2-\omega_3-\omega_s;n\omega_{\mathrm{rep},1})\tilde{\mathcal{E}}_2(\omega_2;m\omega_{\mathrm{rep},2}) \\
\times \tilde{\mathcal{E}}_1^*(\omega_3;r\omega_{\mathrm{rep},1})\tilde{\mathcal{E}}_2(\omega_1;p\omega_{\mathrm{rep},2})\delta(n+r-m-p)e^{i(\omega_2+\omega_1)\Delta t} + \tilde{\mathcal{E}}_2^*(\omega_1+\omega_2-\omega_3-\omega_s;m\omega_{\mathrm{rep},2}) \\
\times \tilde{\mathcal{E}}_1(\omega_2;n\omega_{\mathrm{rep},1})\tilde{\mathcal{E}}_2^*(\omega_3;p\omega_{\mathrm{rep},2})\tilde{\mathcal{E}}_1(\omega_1;r\omega_{\mathrm{rep},1})\delta(-n-r+m+p)e^{-i(\omega_1+\omega_2-\omega_s)\Delta t}] \\
\times \chi^{(3)}(-\omega_1-\omega_2+\omega_3;\omega_1,\omega_2,\omega_3). \qquad \text{(A1)}
\end{aligned}$$

We used the fact that the signal is invariant to the exchange of ω_1 and ω_2 in the expressions for the fields $\tilde{\mathcal{E}}_2(\omega_2)\tilde{\mathcal{E}}_1(\omega_1)$. The integrations over ω_1, ω_2 and ω_3 in Eq. (A1) can be done with the help of the δ function in the fields Eq. (19), giving

$$\begin{aligned}
&S^{(3)}_{t1122}(\omega_s;\omega_{\mathrm{rep},1},\omega_{\mathrm{rep},2},\Delta t) \\
&= -\mathcal{I}\frac{2}{\hbar}\{\mathcal{E}^*(n\omega_{\mathrm{rep},1}-\omega_c)\tilde{\mathcal{E}}(m\omega_{\mathrm{rep},2}-\omega_c)\tilde{\mathcal{E}}^*(p\omega_{\mathrm{rep},2}-\omega_c)\tilde{\mathcal{E}}(r\omega_{\mathrm{rep},1}-\omega_c) \\
&\times \delta(n-r-m+p)\delta[(m-p)\omega_{\mathrm{rep},2}+(r-n)\omega_{\mathrm{rep},1}-\omega_s]e^{-i(p-m)\omega_{\mathrm{rep},2}\Delta t} \\
&\times [\chi^{(3)}(-r\omega_{\mathrm{rep},1}-(m-p)\omega_{\mathrm{rep},2};r\omega_{\mathrm{rep},1},m\omega_{\mathrm{rep},2},p\omega_{\mathrm{rep},2}) \\
&+ \chi^{(3)}(-r\omega_{\mathrm{rep},1}-(m-p)\omega_{\mathrm{rep},2};m\omega_{\mathrm{rep},2},r\omega_{\mathrm{rep},1},p\omega_{\mathrm{rep},2})] + \mathcal{E}_2^*(m\omega_{\mathrm{rep},2}-\omega_c) \\
&\times \tilde{\mathcal{E}}_1(n\omega_{\mathrm{rep},1}-\omega_c)\tilde{\mathcal{E}}_1^*(r\omega_{\mathrm{rep},1}-\omega_c)\tilde{\mathcal{E}}_2(p\omega_{\mathrm{rep},2}-\omega_c)\delta(-n+r+m-p) \\
&\times \delta[(n-r)\omega_{\mathrm{rep},1}-(m-p)\omega_{\mathrm{rep},2}-\omega_s]e^{-i[(n-r)\omega_{\mathrm{rep},1}-\omega_s]\Delta t}\} \\
&\times [\chi^{(3)}(-p\omega_{\mathrm{rep},2}-(n-r)\omega_{\mathrm{rep},1};p\omega_{\mathrm{rep},2},n\omega_{\mathrm{rep},1},r\omega_{\mathrm{rep},1}) \\
&+ \chi^{(3)}(-p\omega_{\mathrm{rep},2}-(n-r)\omega_{\mathrm{rep},1};n\omega_{\mathrm{rep},1},p\omega_{\mathrm{rep},2},r\omega_{\mathrm{rep},1})] + \mathcal{E}_1^*(n\omega_{\mathrm{rep},1}-\omega_c)\tilde{\mathcal{E}}_2(m\omega_{\mathrm{rep},2}-\omega_c) \\
&\times \tilde{\mathcal{E}}_1^*(r\omega_{\mathrm{rep},1}-\omega_c)\tilde{\mathcal{E}}_2(p\omega_{\mathrm{rep},2}-\omega_c)\delta(n+r-m-p)\delta[(m+p)p\omega_{\mathrm{rep},2}-(r+n)\omega_{\mathrm{rep},1}-\omega_s] \\
&\times e^{i(m+p)\omega_{\mathrm{rep},2}\Delta t}\chi^{(3)}(-(p+m)\omega_{\mathrm{rep},2}+r\omega_{\mathrm{rep},1};p\omega_{\mathrm{rep},2},m\omega_{\mathrm{rep},2},r\omega_{\mathrm{rep},1}) \\
&+ \mathcal{E}_2^*(m\omega_{\mathrm{rep},2}-\omega_c)\tilde{\mathcal{E}}_1(n\omega_{\mathrm{rep},1}-\omega_c)\tilde{\mathcal{E}}_2^*(p\omega_{\mathrm{rep},2}-\omega_c)\tilde{\mathcal{E}}_1(r\omega_{\mathrm{rep},1}-\omega_c)\delta(-n-r+m+p) \\
&\times \delta[(n+r)\omega_{\mathrm{rep},1}-(m+p)\omega_{\mathrm{rep},2}-\omega_s]e^{-i[(n+r)\omega_{\mathrm{rep},1}-\omega_s]\Delta t} \\
&\times \chi^{(3)}(-(r+n)\omega_{\mathrm{rep},1}+p\omega_{\mathrm{rep},2};r\omega_{\mathrm{rep},1},n\omega_{\mathrm{rep},1},p\omega_{\mathrm{rep},2}). \qquad \text{(A2)}
\end{aligned}$$

The last two δ functions can be used to eliminate two summations, giving

$$S^{(3)}_{t1122}(\omega_s;\Delta t,\delta\omega_{\mathrm{rep}},\omega_{\mathrm{rep},1}) = \sum_{n,m}^{N} S^{(3)}_{t1122}\left(\omega_s;\Delta t,\delta\omega_{\mathrm{rep}},\omega_{\mathrm{rep},1},n,m,\frac{m\delta\omega_{\mathrm{rep}}-\omega_s}{\omega_{\mathrm{rep},1}},\frac{n\delta\omega_{\mathrm{rep}}-\omega_s}{\omega_{\mathrm{rep},1}}\right), \qquad \text{(A3)}$$

where $S^{(3)}_{t1122}(\omega_s)$ is given as

$$\begin{aligned}
&S^{(3)}_{t1122}(\omega_s;\omega_{\mathrm{rep},1},\omega_{\mathrm{rep},2},\Delta t,n,m,p,r) \\
&= -\mathcal{I}\frac{2}{\hbar}[\mathcal{E}^*(n\omega_{\mathrm{rep},1}-\omega_c)\tilde{\mathcal{E}}(m\omega_{\mathrm{rep},2}-\omega_c)\tilde{\mathcal{E}}^*(p\omega_{\mathrm{rep},2}-\omega_c) \\
&\times \tilde{\mathcal{E}}(r\omega_{\mathrm{rep},1}-\omega_c)e^{-i(p-m)\omega_{\mathrm{rep},2}\Delta t}[\chi^{(3)}(-r\omega_{\mathrm{rep},1}-(m-p)\omega_{\mathrm{rep},2};r\omega_{\mathrm{rep},1},m\omega_{\mathrm{rep},2},p\omega_{\mathrm{rep},2}) \\
&+ \chi^{(3)}(-r\omega_{\mathrm{rep},1}-(m-p)\omega_{\mathrm{rep},2};m\omega_{\mathrm{rep},2},r\omega_{\mathrm{rep},1},p\omega_{\mathrm{rep},2})] \\
&+ \mathcal{E}^*(-m\omega_{\mathrm{rep},2}-\omega_c)\tilde{\mathcal{E}}(-n\omega_{\mathrm{rep},1}-\omega_c)\tilde{\mathcal{E}}^*(-r\omega_{\mathrm{rep},1}-\omega_c)\tilde{\mathcal{E}}(-p\omega_{\mathrm{rep},2}-\omega_c) \\
&\times e^{-i[(-n+r)\omega_{\mathrm{rep},1}-\omega_s]\Delta t}[\chi^{(3)}(p\omega_{\mathrm{rep},2}+(n-r)\omega_{\mathrm{rep},1};-p\omega_{\mathrm{rep},2},-n\omega_{\mathrm{rep},1},-r\omega_{\mathrm{rep},1}) \\
&+ \chi^{(3)}(p\omega_{\mathrm{rep},2}+(n-r)\omega_{\mathrm{rep},1};-n\omega_{\mathrm{rep},1},-p\omega_{\mathrm{rep},2},-r\omega_{\mathrm{rep},1})]
\end{aligned}$$

$$+\mathcal{E}^*(n\omega_{\mathrm{rep},1}-\omega_c)\tilde{\mathcal{E}}(m\omega_{\mathrm{rep},2}-\omega_c)\tilde{\mathcal{E}}^*(-r\omega_{\mathrm{rep},1}-\omega_c)\tilde{\mathcal{E}}(-p\omega_{\mathrm{rep},2}-\omega_c)e^{i(m-p)\omega_{\mathrm{rep},2}\Delta t}$$
$$\times\chi^{(3)}((p-m)\omega_{\mathrm{rep},2}+r\omega_{\mathrm{rep},1};-p\omega_{\mathrm{rep},2},m\omega_{\mathrm{rep},2},r\omega_{\mathrm{rep},1})+\mathcal{E}^*(-m\omega_{\mathrm{rep},2}-\omega_c)\tilde{\mathcal{E}}(-n\omega_{\mathrm{rep},1}-\omega_c)$$
$$\times\tilde{\mathcal{E}}^*(p\omega_{\mathrm{rep},2}-\omega_c)\tilde{\mathcal{E}}(r\omega_{\mathrm{rep},1}-\omega_c)e^{-i[-(n-r)\omega_{\mathrm{rep},1}-\omega_s]\Delta t}$$
$$\times\chi^{(3)}((-r+n)\omega_{\mathrm{rep},1}+p\omega_{\mathrm{rep},2};r\omega_{\mathrm{rep},1},-n\omega_{\mathrm{rep},1},p\omega_{\mathrm{rep},2}). \tag{A4}$$

APPENDIX B: TIME-RESOLVED TRANSMISSION SIGNAL $\tilde{\mathcal{E}}_1^3\tilde{\mathcal{E}}_2$

Inserting Eqs. (19) and (25) into the transmission signal Eq. (8), yields

$$S^{(3)}_{t1112}(\omega_s;\omega_{\mathrm{rep},1},\omega_{\mathrm{rep},2},\Delta t)$$
$$=-\mathcal{I}\frac{2}{\hbar}\omega^3_{\mathrm{rep},1}\omega_{\mathrm{rep},2}\int_{-\infty}^{\infty}d\omega_1\int_{-\infty}^{\infty}d\omega_2\int_{-\infty}^{\infty}d\omega_3$$
$$\times[\tilde{\mathcal{E}}_1^*(\omega_1+\omega_2-\omega_3-\omega_s;m\omega_{\mathrm{rep},1})\tilde{\mathcal{E}}_2(\omega_2;p\omega_{\mathrm{rep},2})\tilde{\mathcal{E}}_1^*(\omega_3;r\omega_{\mathrm{rep},1})\tilde{\mathcal{E}}_1(\omega_1;n\omega_{\mathrm{rep},1})$$
$$\times\delta(-n+r+m-p)e^{-i(\omega_2-\omega_3-\omega_s)\Delta t}+\tilde{\mathcal{E}}_1^*(\omega_1+\omega_2-\omega_3-\omega_s;n\omega_{\mathrm{rep},1})\tilde{\mathcal{E}}_1(\omega_2;m\omega_{\mathrm{rep},1})$$
$$\times\tilde{\mathcal{E}}_2^*(\omega_3;p\omega_{\mathrm{rep},2})\tilde{\mathcal{E}}_1(\omega_1;r\omega_{\mathrm{rep},1})\delta(n-r-m+p)e^{i(\omega_2+\omega_1)\Delta t}+\tilde{\mathcal{E}}_1^*(\omega_1+\omega_2-\omega_3-\omega_s;m\omega_{\mathrm{rep},1})$$
$$\times\tilde{\mathcal{E}}_1(\omega_2;n\omega_{\mathrm{rep},1})\tilde{\mathcal{E}}_1^*(\omega_3;r\omega_{\mathrm{rep},1})\tilde{\mathcal{E}}_2(\omega_1;p\omega_{\mathrm{rep},2})\delta(-n+r+m-p)e^{-i(\omega_1+\omega_2-\omega_s)\Delta t}]$$
$$\times\chi^{(3)}(-\omega_1-\omega_2+\omega_3;\omega_1,\omega_2,\omega_3). \tag{B1}$$

We used the fact that the signal is invariant to the exchange of ω_1 and ω_2 in the expressions for the fields $\tilde{\mathcal{E}}_2(\omega_2)\tilde{\mathcal{E}}_1(\omega_1)$. Using the δ functions in the expressions for the fields Eq. (19), the integrations over ω_1, ω_2, and ω_3 in Eq. (B1) are completed, giving

$$S^{(3)}_{t1112}(\omega_s;\omega_{\mathrm{rep},1},\omega_{\mathrm{rep},2},\Delta t,n,m,p,r)$$
$$=-\mathcal{I}\frac{2}{\hbar}\omega^3_{\mathrm{rep},1}\omega_{\mathrm{rep},2}[\tilde{\mathcal{E}}_1^*(m\omega_{\mathrm{rep},1}-\omega_c)\tilde{\mathcal{E}}_2(p\omega_{\mathrm{rep},2}-\omega_c)\tilde{\mathcal{E}}_1^*(r\omega_{\mathrm{rep},1}-\omega_c)\tilde{\mathcal{E}}_1(n\omega_{\mathrm{rep},1}-\omega_c)\delta(-n+r+m-p)$$
$$\times\delta(-p\omega_{\mathrm{rep},1}+p\omega_{\mathrm{rep},2}-\omega_s)e^{-i(p\omega_{\mathrm{rep},2}-r\omega_{\mathrm{rep},1}-\omega_s)\Delta t}$$
$$\times\chi^{(3)}((r-n)\omega_{\mathrm{rep},1}-p\omega_{\mathrm{rep},2};n\omega_{\mathrm{rep},1},p\omega_{\mathrm{rep},2},r\omega_{\mathrm{rep},1})+\tilde{\mathcal{E}}_1^*(n\omega_{\mathrm{rep},1}-\omega_c)$$
$$\times\tilde{\mathcal{E}}_1(m\omega_{\mathrm{rep},1}-\omega_c)\tilde{\mathcal{E}}_2^*(p\omega_{\mathrm{rep},2}-\omega_c)\tilde{\mathcal{E}}_1(r\omega_{\mathrm{rep},1}-\omega_c)\delta(n-r-m+p)$$
$$\times\delta(p\omega_{\mathrm{rep},1}-p\omega_{\mathrm{rep},2}-\omega_s)e^{i(m\omega_{\mathrm{rep},1}+r\omega_{\mathrm{rep},1})\Delta t}\chi^{(3)}(-(r+m)\omega_{\mathrm{rep},1}+p\omega_{\mathrm{rep},2};r\omega_{\mathrm{rep},1},m\omega_{\mathrm{rep},1},p\omega_{\mathrm{rep},2})$$
$$+\tilde{\mathcal{E}}_1^*(m\omega_{\mathrm{rep},1}-\omega_c)\tilde{\mathcal{E}}_1(n\omega_{\mathrm{rep},1}-\omega_c)\tilde{\mathcal{E}}_1^*(r\omega_{\mathrm{rep},1}-\omega_c)\tilde{\mathcal{E}}_2(p\omega_{\mathrm{rep},2}-\omega_c)\delta(-n+r+m-p)$$
$$\times\delta(-p\omega_{\mathrm{rep},1}+p\omega_{\mathrm{rep},2}-\omega_s)e^{-i(p\omega_{\mathrm{rep},2}+n\omega_{\mathrm{rep},1}-\omega_s)\Delta t}$$
$$\times\chi^{(3)}(-p\omega_{\mathrm{rep},2}-(n-r)\omega_{\mathrm{rep},1};p\omega_{\mathrm{rep},2},n\omega_{\mathrm{rep},1},r\omega_{\mathrm{rep},1})]. \tag{B2}$$

The last two δ functions can be used to eliminate two of the summations, giving

$$S^{(3)}_{t1112}(\omega_s;\Delta t,\delta\omega_{\mathrm{rep}},\omega_{\mathrm{rep},1})=\sum_{n,m}^{N}S_t^{(3)}\left(\omega_s;\Delta t,\delta\omega_{\mathrm{rep}},\omega_{\mathrm{rep},1},n,m,\frac{-\omega_s}{\delta\omega_{\mathrm{rep}}},\frac{(n-m)\delta\omega_{\mathrm{rep}}-\omega_s}{\delta\omega_{\mathrm{rep}}}\right), \tag{B3}$$

where $S^{(3)}_{t1112}(\omega_s)$ is given as

$$S^{(3)}_{t1112}(\omega_s;\omega_{\mathrm{rep},1},\omega_{\mathrm{rep},2},\Delta t,n,m,p,r)$$
$$=-\mathcal{I}\frac{2}{\hbar}\omega^3_{\mathrm{rep},1}\omega_{\mathrm{rep},2}[\tilde{\mathcal{E}}_1^*(m\omega_{\mathrm{rep},1}-\omega_c)\tilde{\mathcal{E}}_2(p\omega_{\mathrm{rep},2}-\omega_c)\tilde{\mathcal{E}}_1^*(r\omega_{\mathrm{rep},1}-\omega_c)\tilde{\mathcal{E}}_1(n\omega_{\mathrm{rep},1}-\omega_c)e^{-i(p\omega_{\mathrm{rep},2}-r\omega_{\mathrm{rep},1}-\omega_s)\Delta t}$$
$$\times\chi^{(3)}((r-n)\omega_{\mathrm{rep},1}-p\omega_{\mathrm{rep},2};n\omega_{\mathrm{rep},1},p\omega_{\mathrm{rep},2},r\omega_{\mathrm{rep},1})+\tilde{\mathcal{E}}_1^*(n\omega_{\mathrm{rep},1}-\omega_c)\tilde{\mathcal{E}}_1(m\omega_{\mathrm{rep},1}-\omega_c)$$
$$\times\tilde{\mathcal{E}}_2^*(-p\omega_{\mathrm{rep},2}-\omega_c)\tilde{\mathcal{E}}_1(r\omega_{\mathrm{rep},1}-\omega_c)e^{i(m\omega_{\mathrm{rep},1}+r\omega_{\mathrm{rep},1})\Delta t}$$
$$\times\chi^{(3)}(-(r+m)-p\omega_{\mathrm{rep},2};r\omega_{\mathrm{rep},1},m\omega_{\mathrm{rep},1},-p\omega_{\mathrm{rep},2})+\tilde{\mathcal{E}}_1^*(m\omega_{\mathrm{rep},1}-\omega_c)\tilde{\mathcal{E}}_1(n\omega_{\mathrm{rep},1}-\omega_c)$$
$$\times\tilde{\mathcal{E}}_1^*(r\omega_{\mathrm{rep},1}-\omega_c)\tilde{\mathcal{E}}_2(p\omega_{\mathrm{rep},2}-\omega_c)e^{-i(p\omega_{\mathrm{rep},2}+n\omega_{\mathrm{rep},1}-\omega_s)\Delta t}$$
$$\times\chi^{(3)}(-p\omega_{\mathrm{rep},2}-(n-r)\omega_{\mathrm{rep},1};p\omega_{\mathrm{rep},2},n\omega_{\mathrm{rep},1},r\omega_{\mathrm{rep},1})]. \tag{B4}$$

[1] T. Udem, J. Reichert, R. Holzwarth, and T. W. Hänsch, Opt. Lett. **24**, 881 (1999).
[2] S. T. Cundiff and J. Ye, Rev. Mod. Phys. **75**, 325 (2003).
[3] T. Wilken, G. L. Curto, R. A. Probst, T. Steinmetz, A. Manescau, L. Pasquini, J. I. González Hernández, R. Rebolo, T. W. Hänsch, T. Udem, and R. Holzwarth, Nature (London) **485**, 611 (2012).
[4] T. Ideguchi, S. Holzner, B. Bernhardt, G. Guelachvili, N. Picqué, and T. W. Hänsch, Nature (London) **502**, 355 (2013).
[5] I. Barmes, S. Witte, and K. S. E. Eikema, Phys. Rev. Lett. **111**, 023007 (2013).
[6] I. Barmes, S. Witte, and K. S. E. Eikema, Nat. Photon. **7**, 38 (2013).
[7] A. M. Weiner, Nat. Photon. **7**, 6 (2013).
[8] P. Giaccari, J.-D. Deschênes, P. Saucier, J. Genest, and P. Tremblay, Opt. Express **16**, 4347 (2008).
[9] F. Krausz and M. Ivanov, Rev. Mod. Phys. **81**, 163 (2009).
[10] J. Ye and S. T. Cundiff, *Femtosecond Optical Frequency Comb: Principle, Operation and Applications* (Springer, New York, 2005).
[11] F. Keilmann and S. Amarie, J. Infrared Milli. Terahz. Waves **33**, 479 (2012).
[12] A. Schliesser, N. Picqué, and T. W. Hänsch, Nat. Photon. **6**, 440 (2012).
[13] B. Bernhardt, A. Ozawa, P. Jacquet, M. Jacquey, Y. Kobayashi, T. Udem, R. Holzwarth, G. Guelachvili, T. W. Hänsch, and N. Picqué, Nat. Photon. **4**, 55 (2010).
[14] I. Coddington, W. C. Swann, and N. R. Newbury, Phys. Rev. Lett. **100**, 013902 (2008).
[15] I. Coddington, W. C. Swann, and N. R. Newbury, Phys. Rev. A **82**, 043817 (2010).
[16] S. A. Diddams, D. J. Jones, J. Ye, S. T. Cundiff, J. L. Hall, J. K. Ranka, R. S. Windeler, R. Holzwarth, T. Udem, and T. W. Hänsch, Phys. Rev. Lett. **84**, 5102 (2000).
[17] T. W. Hänsch and N. Picqué, J. Phys.: Conf. Ser. **467**, 012001 (2013).
[18] F. Adler, P. Maslowski, A. Foltynowicz, K. C. Cossel, T. C. Briles, I. Hartl, and J. Ye, Opt. Express **18**, 21861 (2010).
[19] T. Ideguchi, A. Poisson, G. Guelachvili, N. Picqué, and T. W. Hänsch, Nat. Commun. **5**, 3375 (2014).
[20] A. Foltynowicz, T. Ban, P. Maslowski, F. Adler, and J. Ye, Phys. Rev. Lett. **107**, 233002 (2011).
[21] E. Baumann, F. R. Giorgetta, W. C. Swann, A. M. Zolot, I. Coddington, and N. R. Newbury, Phys. Rev. A **84**, 062513 (2011).
[22] E. S. B. Bernhardt, Appl. Phys. B **100**, 3 (2010).
[23] T. Ideguchi, B. Bernhardt, G. Guelachvili, T. W. Hänsch, and N. Picqué, Opt. Lett. **37**, 4498 (2012).
[24] F. Ferdous, H. Miao, D. E. Leaird, K. Srinivasan, J. Wang, L. Chen, L. T. Varghese, and A. M. Weiner, Nat. Photon. **5**, 770 (2011).
[25] X. Zhou, X. Zheng, H. Wen, H. Zhang, and B. Zhou, Opt. Lett. **38**, 5331 (2013).
[26] A. Rashidinejad and A. M. Weiner, in *Proceedings of CLEO: 2013*, OSA Technical Digest (Optical Society of America, Washington, D.C., 2013), p. CTu3G.4.
[27] S. T. Cundiff and A. M. Weiner, Nat. Photon. **4**, 760 (2010).
[28] S. Mukamel, *Principles of Nonlinear Optical Spectroscopy* (Oxford University Press, New York, 1995).
[29] K. E. Dorfman and S. Mukamel, New J. Phys. **16**, 033013 (2014).
[30] J. Rauschenberger, T. Fortier, D. Jones, J. Ye, and S. Cundiff, Opt. Express **10**, 1404 (2002).
[31] K. Holman, R. Jones, A. Marian, S. Cundiff, and J. Ye, IEEE J. Sel. Top. Quantum Electron. **9**, 1018 (2003).
[32] D. J. Jones, S. A. Diddams, J. K. Ranka, A. Stentz, R. S. Windeler, J. L. Hall, and S. T. Cundiff, Science **288**, 635 (2000).
[33] D. P. Hoffman, D. Valley, S. R. Ellis, M. Creelman, and R. A. Mathies, Opt. Express **21**, 21685 (2013).
[34] F. Quinlan, C. Williams, S. Ozharar, S. Gee, and P. Delfyett, J. Lightwave Technol. **26**, 2571 (2008).
[35] M. Nakazawa, K. Kasai, and M. Yoshida, Opt. Lett. **33**, 2641 (2008).
[36] N. Metropolis and S. Ulam, J. Am. Stat. Assoc. **44**, 335 (1949).
[37] H. L. Anderson, Los Alamos Science **14**, 96 (1986).
[38] Z. Jiang, D. S. Seo, D. E. Leaird, and A. M. Weiner, Opt. Lett. **30**, 1557 (2005).
[39] N. K. Fontaine, R. P. Scott, J. Cao, A. Karalar, W. Jiang, K. Okamoto, J. P. Heritage, B. H. Kolner, and S. J. B. Yoo, Opt. Lett. **32**, 865 (2007).
[40] Z. Jiang, C.-B. Huang, D. E. Leaird, and A. M. Weiner, Nat. Photon. **1**, 463 (2007).